Earthquake Engineering & Structural Dynamics

WILEY

RESEARCH ARTICLE OPEN ACCESS

Weak-Story Mitigation and Drift Redistribution in Moment-Resisting Frames Using Stepping Rocking Walls

Mehrdad Aghagholizadeh

Department of Civil and Environmental Engineering, Loyola Marymount University, Los Angeles, California, USA

Correspondence: Mehrdad Aghagholizadeh (mehrdad.aghagholizadeh@lmu.edu)

Received: 12 December 2025 | **Revised:** 16 May 2026 | **Accepted:** 28 May 2026

Keywords: repairability | rocking walls | seismic retrofit | structural resilience | weak-story mitigation

ABSTRACT

This study investigates the seismic response of moment-resisting frames retrofitted with a stepping rocking wall, with emphasis on weak-story mitigation and residual drift reduction under both ordinary and pulse-like ground motions. Nonlinear response-history analyses are conducted on 9-story and 20-story SAC Los Angeles frames. The results show that the unretrofitted frames develop concentrated drift demands and significant residual deformations, particularly in the taller system. Introducing the stepping rocking wall modifies this behavior by enabling uplift and recentering, which promotes a first-mode-dominated response and suppresses higher-mode-induced drift concentration. As a result, story drift demands are redistributed along the height, reducing drift concentration and limiting the formation of weak-story mechanisms. To quantify this effect, a drift concentration factor (DCF) is employed as a scalar measure of drift localization across ground motions, addressing the limitation of peak story drift as a global response metric. The results show consistently lower DCF values in the retrofitted systems, confirming reduced drift localization and improved deformation distribution. Additional analyses using pulse-like ground motions scaled to the maximum considered earthquake (MCE) level show that these beneficial trends persist under increased shaking intensity, with substantial reductions in peak interstory drift, residual drift, and drift concentration in both buildings. The findings demonstrate that stepping rocking walls not only reduce peak and residual demands, but also fundamentally alter the distribution of seismic deformation, providing a mechanism for mitigating weak-story behavior and improving post-earthquake repairability.

1 | Introduction

Near-fault pulse-like ground motions that contain coherent acceleration and velocity pulses can impose large lateral deformation demands on buildings [1–4]. These motions often produce concentrated drift in only a few stories and can trigger weak-story mechanisms, as seen after the 1971 San Fernando, California, 1994 Northridge, California, and 1995 Kobe, Japan earthquakes. When deformation localizes, the resulting soft story behavior leads to severe structural and nonstructural damage and can limit post-earthquake operability even when global stability is not fully lost. Examples of such failures are shown in Figure 1a–c.

Traditional methods for mitigating weak-story behavior often rely on adding stiff shear walls or core systems [5–9]. Although effective at limiting drift, these walls can experience significant cyclic degradation concentrated near their base under long-duration or long-period shaking (Figure 1a), and may be subjected to large ductility demands under near-fault pulses. Such damage can compromise post-earthquake operability and lead to extended downtime.

Residual drift is a particularly important indicator of repairability. Following the 2010 Canterbury and 2011 Christchurch, New Zealand earthquakes, many buildings with residual drift greater

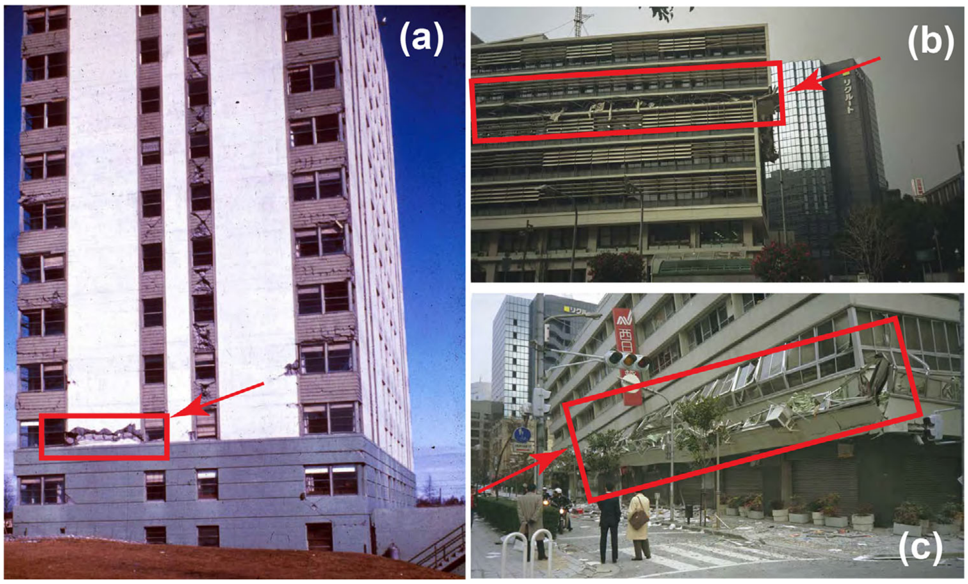

FIGURE 1 | (a) A 14-story reinforced concrete apartment building in Anchorage, Alaska, severely damaged during the 1964 Alaska earthquake.(Image courtesy of the USGS [10]). (b,c) Weak-story failure in the upper stories of buildings following the 1995 Kobe, Japan earthquake. (Images courtesy of the NOAA [11]).

than about 0.5% were demolished because repair was not economically viable [12–15]. Despite the importance of this response measure, current seismic provisions, ASCE 7-22 (Minimum Design Loads and Associated Criteria for Buildings and Other Structures), do not explicitly limit residual drift for most new buildings [16], and ASCE 41 (Seismic Evaluation and Retrofit of Existing Buildings) does not require residual drift checks when evaluating or retrofitting existing structures [17]. As a result, existing moment-resisting frames (MRFs), especially taller and more flexible ones, remain vulnerable to drift concentration and permanent deformation when subjected to long period pulses.

Rocking systems provide an alternative approach to controlling deformation by allowing uplift and rotation, which shifts part of the lateral response from plastic curvature to rigid body motion. Housner [18] first described the fundamental mechanics of uplift permitted blocks. Later, Kelly et al. [19, 20] and Meek [21] introduced rocking walls and uplift tolerant core wall behavior that relied on gravity to provide geometric recentering. The PRESSS program [22–25] formalized the concept of controlled rocking and self centering for precast walls. Numerous experimental and analytical studies have since shown that rocking walls, whether prestressed or partially prestressed, can sustain large lateral displacements with very small residual drift [26–43]. More recent developments have extended rocking behavior to steel braced frames, propped and controlled rocking configurations, and external dissipative towers [44–53]. Full scale shake table tests, including the NHERI TallWood building, further confirmed that rocking systems can produce stable hysteresis, predictable drift profiles, and improved resilience [54–56]. In addition to analytical and experimental developments, several self-centering and rocking-based structural systems have been explored at building scale. These include precast rocking wall systems developed under the PRESSS program [22–25], self-centering steel braced frames, and pin-supported rocking frames implemented in Japan by Qu et al. [37] as a retrofit strategy for existing frame structures. These systems demonstrate that controlled uplift, recentering, and distributed deformation are viable mechanisms for improving seismic performance and mitigating damage concentration.

Although the broader mechanics of rocking systems are well understood, considerably less attention has been given to stepping rocking walls used as retrofit elements for mid and high rise MRFs subjected to recorded near-fault pulses. Prior analytical comparisons of stepping, pinned, and vertically restrained rocking walls [38–40] have shown that unprestressed stepping walls can provide strong geometric recentering without introducing the large foundation forces that arise when vertical tendons are used. This characteristic makes stepping walls attractive for retrofit applications where invasive foundation construction is typically difficult or cost prohibitive.

This study investigates the seismic response of MRFs retrofitted with stepping rocking walls using two benchmark SAC Los Angeles buildings, a 9-story and a 20-story frame, analyzed in both original and retrofitted configurations. While rocking systems have been studied extensively, their application as a retrofit strategy for multi-story frames has not been systematically quantified, particularly with respect to drift localization and weak-story mechanisms under pulse-like ground motions.

The study focuses on system-level mechanisms governing drift redistribution and residual deformation when rocking walls are coupled with flexible frame systems. Since peak story drift alone cannot capture deformation localization, a drift concentration factor (DCF) is introduced as a scalar measure of interstory drift distribution along the height, enabling direct quantification of weak-story tendency beyond conventional peak-based metrics. While normalized drift measures have been used in prior studies to describe global deformation patterns, the formulation adopted here directly relates peak story demand to the height-averaged drift, providing a consistent scalar indicator of weak-story tendency and enabling comparison across systems with different deformation characteristics. The response is further interpreted using residual-drift-based repairability criteria from FEMA P-58. To generalize the observed behavior, transient drift spectra based on symmetric and antisymmetric Ricker pulses are developed to examine the influence of pulse characteristics on drift amplification. The results show that stepping rocking walls suppress higher-mode-induced drift concentration, redistribute deformation along the height, and reduce residual drift, thereby mitigating weak-story behavior in flexible frame systems. These findings provide a mechanics-based basis for evaluating retrofit effectiveness and assessing post-earthquake repairability.

The paper first revisits and compares the primary rocking-wall configurations relevant to retrofit applications and establishes the rationale for using a stepping wall. It then presents the nonlinear modeling framework for the SAC LA buildings and the uplift interface formulation. The subsequent section examines the seismic response of the 9-story and 20-story frames under recorded ordinary and pulse-like ground motions, focusing on drift concentration, residual drift, and FEMA P-58 repairability. The study then develops transient drift spectra using symmetric and antisymmetric Ricker pulses to interpret how pulse period and amplitude influence drift amplification. Additional analyses under pulse-like ground motions scaled to the maximum considered earthquake (MCE) level are presented to examine whether the principal response trends persist under increased shaking intensity. The paper concludes by summarizing the main findings and discussing their implications for retrofit practice.

2 | Comparison of Rocking Walls for Different Configurations

This section compares the primary rocking wall configurations relevant to seismic retrofit applications. In this study, the term "rocking wall" refers to a wall system that undergoes controlled uplift and rotation at its base. Three configurations are considered: (i) stepping rocking walls, in which uplift occurs through successive contact and separation without vertical restraint; (ii) pinned rocking walls, where rotation occurs about a fixed pivot; and (iii) vertically restrained rocking walls, in which uplift is limited by vertical post-tensioning or external restraints.

The comparison emphasizes how each configuration mobilizes gravity, uplift kinematics, and overturning resistance, and clarifies the extent to which recentering arises from geometric nonlinearity versus added vertical restraint. Since this study evaluates mid- and high-rise MRFs where residual drift, weak-story formation, and post-earthquake operability govern performance, the discussion focuses on the mechanisms that most directly influence those demands.

2.1 | Idealized Single-Degree-of-Freedom Model for Rocking–Wall–Frame Dynamics

Figure 2 summarizes the SDOF idealizations used to represent the lateral response of a yielding frame coupled with (a) a stepping rocking wall and (b) a pinned rocking wall. The lower panels present the corresponding bilinear representations of the frame spring and the wall uplift mechanism, which serve here only to clarify the distinct sources of nonlinearity introduced by each configuration. The simplified SDOF representation is used solely to illustrate the fundamental rocking mechanism and the interaction between frame yielding and wall uplift. All results presented in this study are obtained from detailed multi-degree-of-freedom models of the 9-story and 20-story frames.

For conceptual purposes, the rocking wall is idealized as a rigid body characterized by size $R = \sqrt{b^2 + h^2}$ and slenderness $\tan\alpha = b/h$, with lateral displacement $u(t)$ related to rotation $\theta(t)$ through geometry [39]. This assumption is commonly adopted in simplified rocking formulations and is most appropriate when wall deformation remains small relative to rigid-body rotation. The effects of wall flexibility are not explicitly represented in this idealization. The frame bilinear response is represented using a Bouc–Wen model [57, 58], expressed as

$$F_s(t) = a k_1 u(t) + (1 - a) k_1 u_y\, z(t), \tag{1}$$

$$\dot{z}(t) = \frac{1}{u_y}\left[\dot{u}(t) - \beta \dot{u}(t)|z(t)|^n - \gamma|\dot{u}(t)|z(t)|z(t)|^{n-1}\right], \tag{2}$$

where k_1, u_y, a, β, γ, and n govern the hysteretic response [59].

Although closed-form equations of motion for both stepping and pinned rocking walls have been derived in prior studies [38–40], they are not repeated here. The focus is instead on the parameters that distinguish the two systems, including self-weight, uplift geometry, and inertial coupling, since these govern the multi-story behavior examined in the subsequent sections. The purpose of this subsection is to clarify the recentering and energy dissipation mechanisms that underpin the building-scale responses evaluated in this study.

2.2 | Comparison of Stepping and Pinned Rocking Wall Configurations

The stepping rocking wall (Figure 2a) rocks about alternating corners, and the change in pivot introduces impact-related energy dissipation. In contrast, the pinned rocking wall (Figure 2b) rotates about a fixed pin, eliminating corner impacts but fundamentally altering how gravity contributes to stability.

For a stepping wall rotating about a corner, the rotational equilibrium may be expressed as [39]

$$\begin{aligned} I\ddot{\theta} = &-\left(m_s(\ddot{u} + \ddot{u}_g) + c\dot{u} + F_s\right) R\cos(\alpha - \theta) \\ &\underbrace{-m_w g R \sin(\alpha - \theta)}_{\text{restoring due to self-weight}} - m_w \ddot{u}_g R\cos(\alpha - \theta), \end{aligned} \tag{3}$$

where $I = \frac{4}{3} m_w R^2$ is the moment of inertia about the pivot, $u = R\left[\sin\alpha - \sin(\alpha - \theta)\right]$ is the horizontal displacement of the oscillator, and $\ddot{u}_g$ is the ground acceleration. The self-weight term in Equation (3) provides a restoring moment that promotes recentering and limits residual drift.

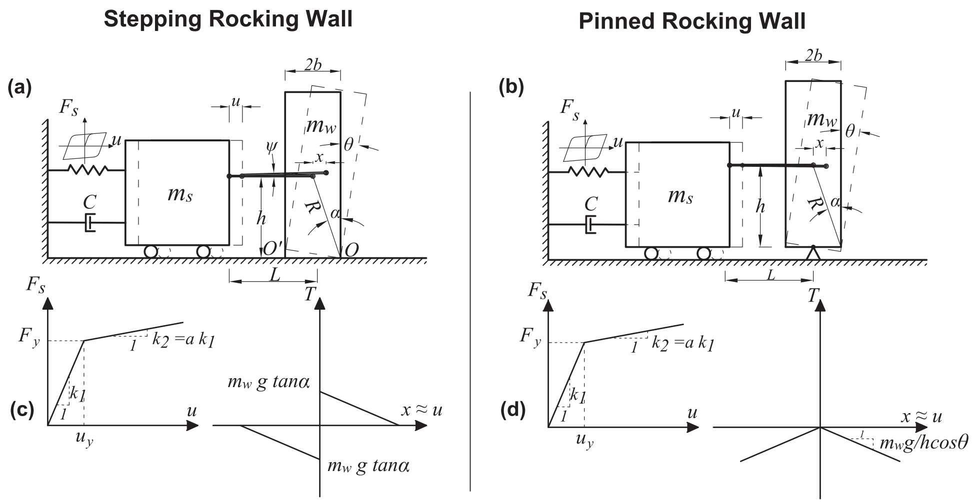

FIGURE 2 | Top row: Yielding SDOF oscillator coupled with (a) a stepping rocking wall and (b) a pinned rocking wall. Bottom row: Bilinear idealizations for (c) the nonlinear frame spring and (d) the wall force–displacement response.

For a pinned rocking wall, the corresponding rotational equilibrium is [38]

$$I\ddot{\theta} = -\left(m_s(\ddot{u} + \ddot{u}_g) + c\dot{u} + F_s\right) h \cos\theta + \underbrace{m_w g h \sin\theta}_{\text{destabilizing due to self-weight}} - m_w \ddot{u}_g h \cos\theta, \quad (4)$$

with $I = m_w R^2 \left(1/3 + \cos^2\alpha\right)$ about the pin and $u = h \sin\theta$ as the horizontal displacement. Here, the gravity term acts in the opposite direction relative to the stepping case, reducing stability and eliminating geometric recentering.

These contrasting gravity effects underpin the different behaviors observed in displacement spectra [38]. Stepping walls suppress peak and residual deformations across a broad period range, particularly for heavier walls, whereas pinned walls tend to amplify demands under similar conditions.

For these reasons, the stepping configuration is adopted as the retrofit system for the multi-story MRFs analyzed in this study, where post-earthquake functionality and drift control are critical.

2.3 | Vertically Restrained Stepping Rocking Walls

A second configuration considered in the literature involves restraining a stepping rocking wall with vertical tendons (Figure 3). The tendon, of axial stiffness EA and possible prestress P_0, increases the vertical stiffness of the wall and suppresses sliding, while also modifying the effective lateral stiffness of the rocking system. As shown in [60, 61], increasing EA gradually shifts the tangent stiffness of the rocking response from negative to positive; therefore, if negative stiffness is part of the design intent, the amount of vertical reinforcement must remain limited. The full governing equation for the vertically restrained wall coupled with a nonlinear SDOF oscillator is provided in [40].

Figure 4 illustrates representative time-history responses for a nonlinear SDOF system with and without vertical restraint. In both example records, the stepping wall enables the oscillator to recenter effectively and substantially reduces residual and peak displacements compared with the bare system. Adding a stiff, prestressed tendon ($(P_0/(m_w g) = 0.5, EA/(m_w g) = 200)$) produces only marginal additional reduction in peak displacement relative to the unrestrained wall, but it significantly increases the normal reactions at the pivoting corners. These elevated reactions raise the likelihood of local crushing or damage at the wall–foundation interface and may render such designs impractical for retrofit applications.

Consistent with the broader parametric results reported in [39], for the medium-rise retrofit configurations considered in this study, tendons contribute little to lateral recentering or drift reduction and impose substantial additional demands on the foundation anchorage. For these reasons, the retrofit strategy adopted in the subsequent multi-story analyses focuses on stepping rocking walls.

3 | Numerical Modeling of Multi-Story MRFs Coupled With Stepping Rocking Walls

This section presents the nonlinear numerical models used to evaluate the seismic response of two benchmark steel MRFs, a 9-story and a 20-story structure from the SAC Phase II Project [62]. Motivated by the mechanisms discussed in Section 2, both buildings are retrofitted with stepping rocking walls, which provide geometric recentering without the foundation demands associated with pinned or vertically restrained alternatives.

All analyses are conducted in OpenSees [63] using nonlinear fiber-based frame elements to capture member yielding, together with an explicit rocking-interface model for the wall uplift, impact, and energy dissipation mechanisms. The modeling framework is intended to capture the key response features of the retrofitted frames, including member yielding, uplift and impact at the wall interface, and the resulting story drift and residual displacement demands under the selected ground motions.

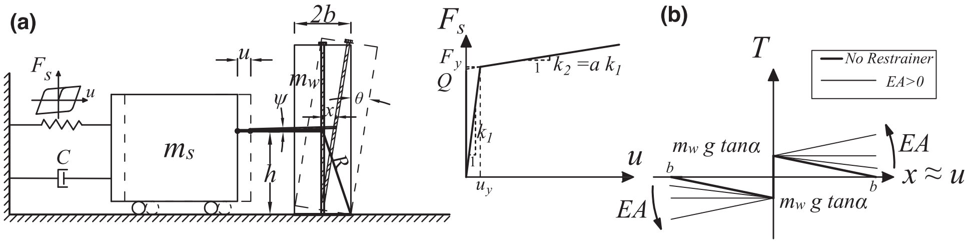

FIGURE 3 | (a) Idealized single-degree-of-freedom (SDOF) oscillator coupled with a vertically restrained stepping rocking wall equipped with a vertical tendon of axial stiffness EA and optional prestress P_0. (b) Bilinear idealization of the nonlinear spring and corresponding force–rotation diagram for the vertically restrained wall.

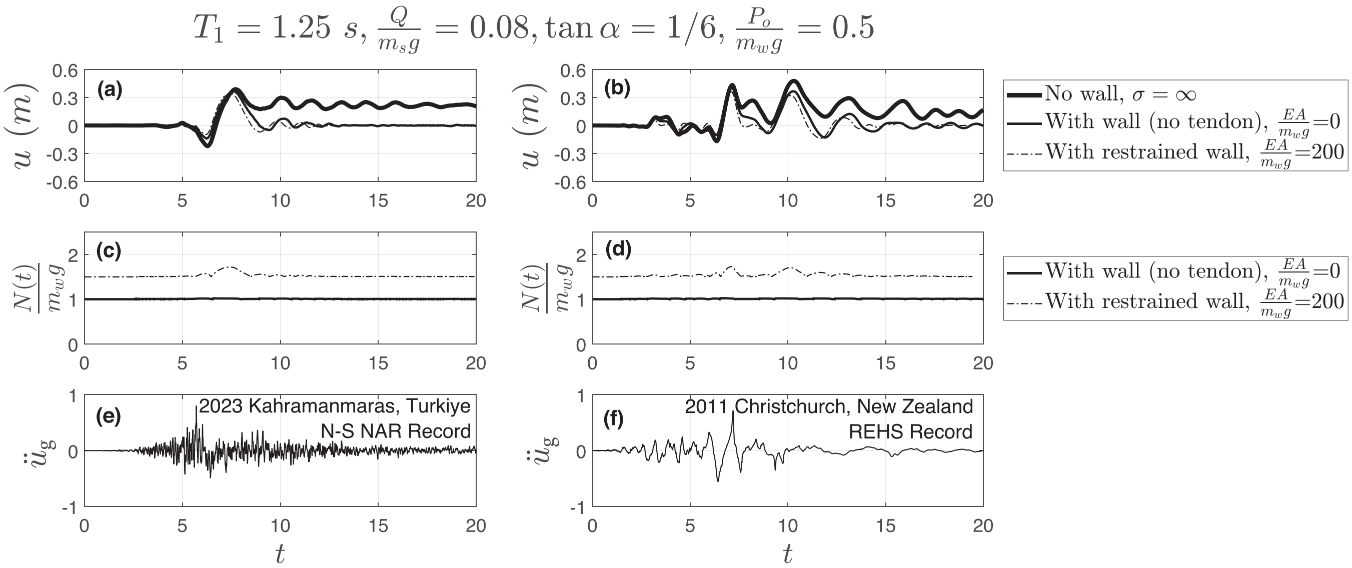

FIGURE 4 | Time-history responses (a,b) and normal forces at the pivoting corners (c,d) of a nonlinear SDOF system with a stepping rocking wall, with and without a vertical tendon. The normalized strength is $Q/m_s = 0.08g$. The input records are (e) the 2023 Kahramanmaras (NAR station), Turkiye and (f) the 2011 Christchurch (REHS station), New Zealand ground motions.

Nonlinear beam-column elements with distributed plasticity are used to capture member yielding. The frame elements are modeled using a linear geometric transformation, while geometric nonlinearity associated with large displacements is explicitly captured in the rocking wall through a corotational formulation. Panel zone deformations are not modeled explicitly, and their influence is implicitly included in the global frame response. Strength and stiffness degradation effects are not explicitly modeled. Gravity loads are represented through lumped masses at each floor level, and a leaning-column formulation is not employed, consistent with standard SAC modeling assumptions. These modeling assumptions may influence residual drift predictions and should be considered when interpreting the results.

The rocking wall is coupled to the frame through lateral compatibility at each floor level, such that floor displacements are shared between the frame and the wall.

The modeling assumptions adopted in this study are intentionally simplified to isolate the dominant system-level response mechanisms associated with rocking behavior. The objective is not to capture detailed component-level deterioration or local damage effects, but rather to provide a consistent framework for comparing the global response of the bare and retrofitted systems.

3.1 | Building Models

The building models are based on the well-documented SAC Phase II steel buildings [62], which have been widely used for nonlinear response-history analyses and benchmarking [64–66]. Elevation and plan views of both frames are shown in Figure 5. All perimeter moment frames in the principal direction of interest are modeled explicitly. Gravity frames are included in the mass distribution but do not contribute to lateral resistance, consistent with SAC conventions.

The 9-story frame (Figure 5a and b) has a total height of 37.17 m and a 45.73 × 45.73 m^2 footprint. The vertical configuration consists of one basement level (3.65 m), one ground floor (5.49 m), and eight upper stories (3.96 m each). Beams and columns are modeled using force-based fiber elements with the `Steel01` material. Floor masses account for structural steel, slabs, partitions, mechanical and electrical systems, and the roof penthouse.

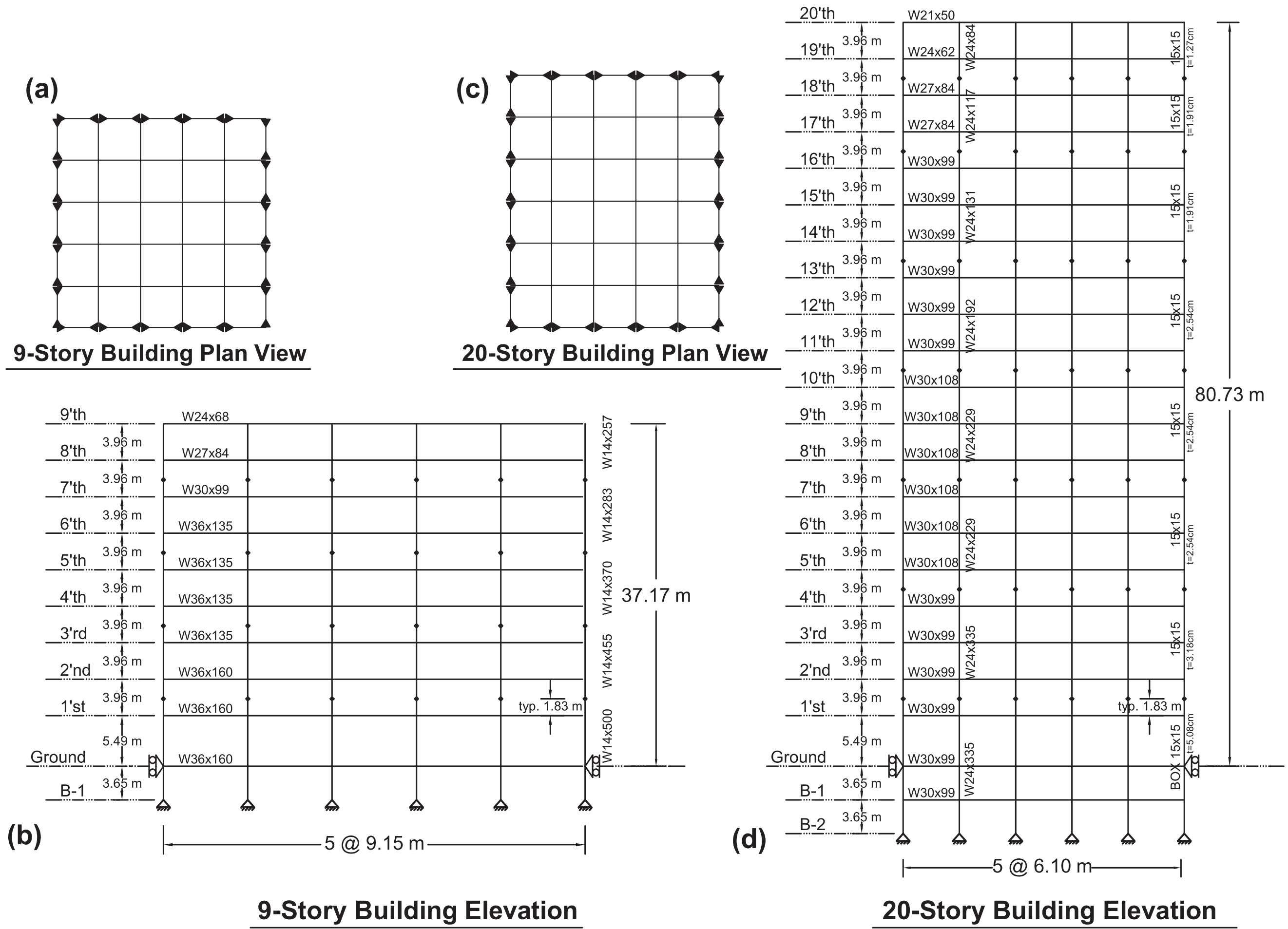

FIGURE 5 | Plan and elevation views of the (a,b) 9-story and (c,d) 20-story steel moment-resisting frames designed for the SAC Phase II Project. Plan views show the locations of perimeter moment-resisting frames (solid triangles) and gravity framing.

The first three vibration periods are 2.26, 0.874, and 0.488 s, consistent with prior SAC studies [64–66].

The 20-story frame (Figure 5c and d) has plan dimensions of 36.58 × 30.48 m^2 and a total height of 80.73 m. The structure includes two basement levels (3.65 m each), a ground floor (5.49 m), and nineteen upper stories (3.96 m each). As in the 9-story building, the perimeter frames provide lateral resistance, while interior framing functions as the gravity system. Beam and column members are modeled as force-based fiber sections with `Steel01` material, and column sizes taper from heavy W-shapes at the base to lighter sections toward the roof. The first three vibration periods are 3.83, 1.33, and 0.769 s, matching published SAC data [64–66].

The modeling approach follows established SAC benchmark practices and is intended to capture global response quantities such as story drift and residual deformation. Local connection behavior and deterioration mechanisms are not explicitly modeled, and the results should therefore be interpreted in terms of global structural response rather than detailed component-level damage.

3.2 | Modeling of Stepping Rocking Walls

To isolate the effect of rocking behavior without additional recentering or supplemental energy dissipation, the retrofit uses stepping rocking walls without tendons or dampers. Each wall is modeled as a monolithic elastic rocking wall with an uplift interface at the base. The wall is modeled with distributed elastic stiffness (EI), while the dominant nonlinear behavior is governed by uplift and compression-only contact at the base interface rather than distributed inelastic deformation along the wall height; local toe crushing effects are therefore not explicitly modeled. A zero-length fiber section employing the elastic-no-tension (`ENT`) material [67, 68] is assigned at the wall-foundation interface to enforce compression-only contact and uplift separation. The compression branch is modeled as linear elastic with stiffness representative of contact behavior at the bearing surface, while tensile resistance is set to zero to permit uplift and separation. This formulation, validated in prior finite-element studies of rocking systems [67, 68], directly captures rocking rotation, gravity-stabilizing moments, and impact-related force transfer at the corners without introducing additional constitutive complexity.

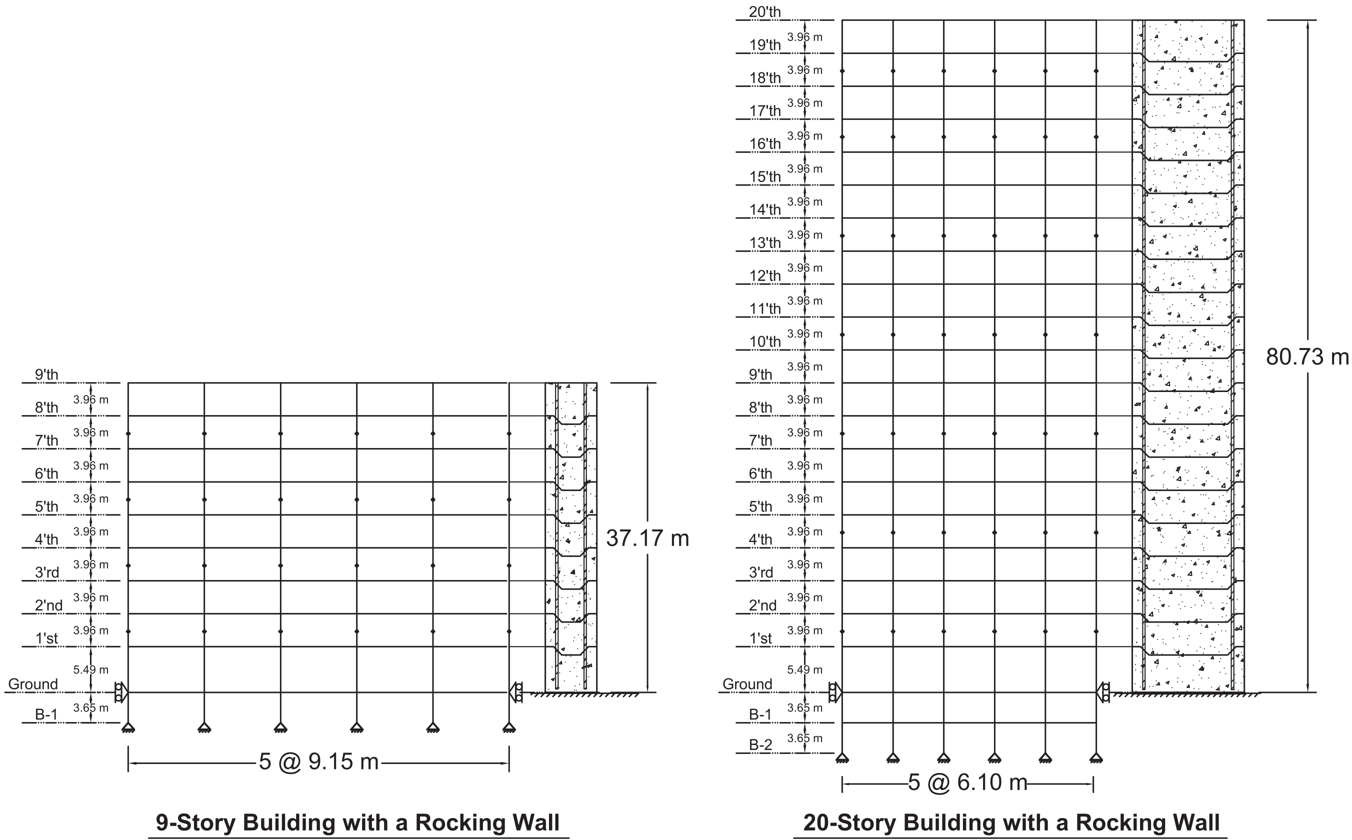

FIGURE 6 | Elevation views of the 9-story and 20-story steel moment-resisting frames retrofitted with a stepping rocking wall.

The wall is coupled to the frame through rigid diaphragm action, such that lateral displacements are compatible at each floor level. Under this assumption, the system-level response is governed by the interaction between the wall and frame and is not strongly dependent on the wall location in plan at the level of idealized modeling considered here. Potential wall flexibility effects and local toe deformation are not explicitly modeled; these may influence the response of slender rocking walls under large uplift demands and are acknowledged as a limitation of the present approach.

For the 9-story MRF retrofit, a wall height of 37.17 m and a wall width of 6.20 m are adopted, corresponding to a width-to-height ratio of approximately $\tan\alpha \approx 1/6$. For the 20-story building, the wall height is 80.73 m and the wall width is 8.0 m, yielding $\tan\alpha \approx 1/10$. These geometries are selected to be compatible with the overall dimensions and aspect ratios of the buildings (shown in Figure 6). The adopted aspect ratios are consistent with typical rocking-wall configurations and are chosen to ensure stable rocking behavior and appropriate interaction with the frame system. The corresponding mass ratios, defined as $\gamma = m_s/m_w$, are $\gamma \approx 10$ for the 9-story frame, and $\gamma \approx 5$ for the 20-story frame.

Although modeled as monolithic, the proposed walls may be constructed as modular precast wall segments. Segmentation improves constructability and quality control through factory fabrication and on-site assembly, allows the optional addition of post-tensioning tendons for stiffness tuning, and facilitates replacement of damaged modules, thereby improving sustainability. From a construction standpoint, the stepping rocking wall requires no tensile anchorage to the foundation, since the rocking mechanism relies on compression-only bearing contact. This distinguishes it from fixed-base shear wall retrofits, which require moment-resisting foundation connections to transfer overturning demands, and suggests potential advantages in retrofit scenarios where invasive foundation modifications are constrained. The system-level feasibility of such an approach is consistent with the pin-supported wall retrofit documented by Qu et al. [37], in which post-tensioned concrete walls were installed within an existing eleven-story frame, connected to floor beams through horizontal trusses, and supported on pin bearings that transfer shear without tensile anchorage to the foundation. The stepping wall proposed here adopts a similar compression-based load transfer mechanism, although its detailed implementation differs and has not been explicitly validated in practice.

3.3 | Ground Motion Selection and Scaling

Because the SAC archetype frames represent buildings in the Los Angeles region, the ground-motion suite is selected and scaled to a Los Angeles-type seismic hazard. The design-basis earthquake (DBE) spectrum is defined according to ASCE 7-22 for Site Class D and Risk Category II, using spectral parameters obtained from the ASCE Hazard Tool [70]. The site-specific values are $S_S = 2.23\,g$ and $S_1 = 0.73\,g$, which give $S_{DS} = 1.51\,g$ and $S_{D1} = 1.11\,g$. Each ground motion is scaled so that its 5%-damped elastic pseudo-spectral acceleration (PSA) at the first-mode period of the corresponding frame matches the DBE target.

TABLE 1 | Ground motions selected from the PEER NGA-West2 database [69], together with the scaling factors used for the 9-story ($\lambda_i^{(9)}$) and 20-story ($\lambda_i^{(20)}$) frames.

RSN	Earthquake	Year	Station	M_w	Mechanism	$\lambda_i^{(9)}$	$\lambda_i^{(20)}$
Ordinary (Non-pulse-like):							
570	Hualien, Taiwan	1986	SMART1 C00	7.30	Reverse	3.46	3.54
583	Hualien, Taiwan	1986	SMART1 O10	7.30	Reverse	3.65	3.43
584	Hualien, Taiwan	1986	SMART1 O12	7.30	Reverse	3.48	3.79
959	Northridge, CA	1994	Canoga Park – Topanga	6.69	Reverse	2.00	2.37
1101	Kobe, Japan	1995	Amagasaki	6.90	Strike slip	1.73	1.72
1246	Chi-Chi, Taiwan	1999	CHY104	7.62	Rev. oblique	2.55	2.31
3748	Cape Mendocino, CA	1992	Ferndale Fire Station	7.01	Reverse	1.83	1.70
Pulse-like:							
171	Imperial Valley, CA	1979	El Centro – Meloland Geot.	6.53	Strike slip	1.86	1.72
802	Loma Prieta, CA	1989	Saratoga – Aloha Ave	6.93	Rev. oblique	2.78	2.71
803	Loma Prieta, CA	1989	Saratoga – W Valley College	6.93	Rev. oblique	2.16	1.99
1063	Northridge, CA	1994	Rinaldi Receiving Sta	6.69	Reverse	1.04	1.01
1084	Northridge, CA	1994	Sylmar – Converter Sta	6.69	Reverse	0.88	0.82
1120	Kobe, Japan	1995	Takatori	6.90	Strike slip	0.71	0.64
1528	Chi-Chi, Taiwan	1999	TCU101	7.62	Rev. oblique	3.25	3.20

For each selected record (listed in Table 1, with acceleration time-histories shown in Figure 7), the 5%-damped PSA spectrum $S_{a,i}(T)$ is computed by combining the two horizontal components using the SRSS method. The first-mode periods of the 9-story and 20-story frames are $T_1^{(9)} = 2.26$ s and $T_1^{(20)} = 3.83$ s, which correspond to target spectral accelerations $S_a^{\mathrm{DBE}}(T_1^{(9)}) = 0.49g$ and $S_a^{\mathrm{DBE}}(T_1^{(20)}) = 0.29g$ based on $S_{D1} = 1.11g$.

The scaling factors for ground motion i are therefore

$$\lambda_i^{(9)} = \frac{0.49g}{S_{a,i}(2.26\ \mathrm{s})}, \qquad \lambda_i^{(20)} = \frac{0.29g}{S_{a,i}(3.83\ \mathrm{s})}. \tag{5}$$

Each horizontal component is multiplied by $\lambda_i^{(9)}$ or $\lambda_i^{(20)}$ depending on the structure being analyzed. The selected ground motions and their corresponding scaling factors are listed in Table 1.

The scaled-record spectra satisfy the ASCE 7-22 DBE target spectrum over the code-required period range $0.2T_1$–$1.5T_1$ for both frames, as shown in Figure 8.

3.4 | Time Integration, Damping, and Analysis Procedure

The numerical modeling framework described above is used for all analyses presented in this section. All simulations are performed using nonlinear finite-element models developed in OpenSees [63], with the frame and rocking wall components modeled as described in Sections 3.1–3.3.

Rocking impacts are modeled using the Hilber–Hughes-Taylor (HHT) method [71] with a dissipation factor $a_d' = -1/3$ and a time step of $\Delta t = 10^{-4}$ s. This dissipative integration scheme has been successfully used in previous finite-element studies of rocking systems [67, 68] to represent impact-induced energy loss without introducing excessive artificial viscous damping.

Additional structural damping is represented using classical Rayleigh damping,

$$\mathbf{C} = \alpha_M \mathbf{M} + \beta_K \mathbf{K}_0, \tag{6}$$

where $\mathbf{M}$ is the mass matrix and $\mathbf{K}_0$ is the initial elastic stiffness matrix. The coefficients α_M and β_K are selected to provide a damping ratio of $\xi = 3\%$ in the first and third vibration modes of each structural model. The use of the initial stiffness matrix avoids artificial increases in damping forces that can arise when tangent stiffness is used in nonlinear analyses. No additional viscous damping is assigned to the uplift interface beyond the numerical dissipation introduced by the HHT integration scheme. Gravity loads are applied incrementally to achieve equilibrium without introducing inaccurate residual drifts. Dynamic response-history analyses are then performed using a base integration step of 10^{-4} s. Krylov–Newton and Newton with line-search algorithms are employed to address convergence difficulties near rocking impacts; if convergence is not achieved, the solution strategy is adaptively adjusted until the ground-motion duration is completed.

Residual drift predictions are sensitive to modeling assumptions, particularly hysteretic behavior and damping representation. The results presented herein are therefore interpreted comparatively to assess relative improvements between configurations, rather than as absolute predictions of residual deformation.

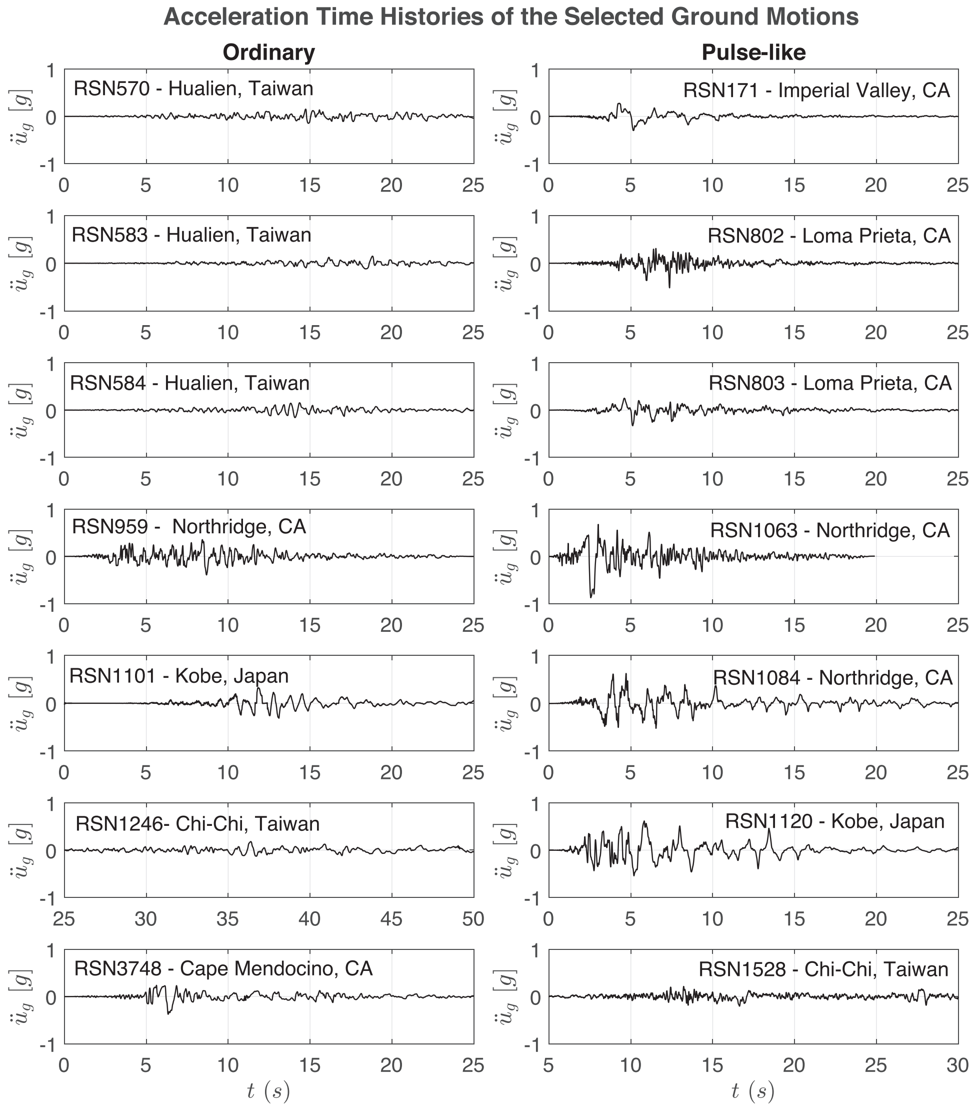

FIGURE 7 | Acceleration time-histories of the 14 selected ground motions from the NGA-West2 database, grouped by ordinary (left) and pulse-like (right) categories.

4 | Time-History Response Under Recorded Ground Motions

This section examines the nonlinear response of the 9-story and 20-story SAC LA MRFs, with and without the stepping rocking-wall retrofit, under the fourteen recorded ground motions described in Section 3.3. Peak floor displacements, peak story drift ratios, and residual story drifts are used to assess weak-story formation and post-earthquake repairability for both ordinary and pulse-like records.

The results presented in this section are obtained from nonlinear response-history analyses using the finite-element models described in Section 3. The observed response is governed by the interaction between frame deformation and rocking-induced uplift at the wall base, which redistributes story drift demands along the height of the structure.

Figures 9–11 summarize the mean response of the 9-story building. The normalized peak displacement profiles in Figure 9 show that, for both ordinary and pulse-like records, the stepping rocking wall produces a more first-mode-dominated shape with reduced roof displacements relative to the bare frame. This indicates that the wall engages the full height of the structure and limits the lateral-offset concentration that typically precedes weak-story behavior.

These trends reflect the fundamental kinematics of the rocking system: by permitting uplift and rotation, the wall introduces a geometric recentering mechanism that constrains lateral deformation to a predominantly first-mode shape. This reduces higher-mode participation and suppresses the localization of story drifts that typically precedes weak-story formation in flexible MRFs.

The corresponding peak story drift profiles in Figure 10 reinforce this trend. For the bare frame, pulse-like motions generate drift concentrations over a limited number of stories, consistent with the development of a weak-story mechanism. In contrast, the retrofitted system exhibits a smoother, nearly linear drift pattern with noticeable reductions in the most highly demanded stories.

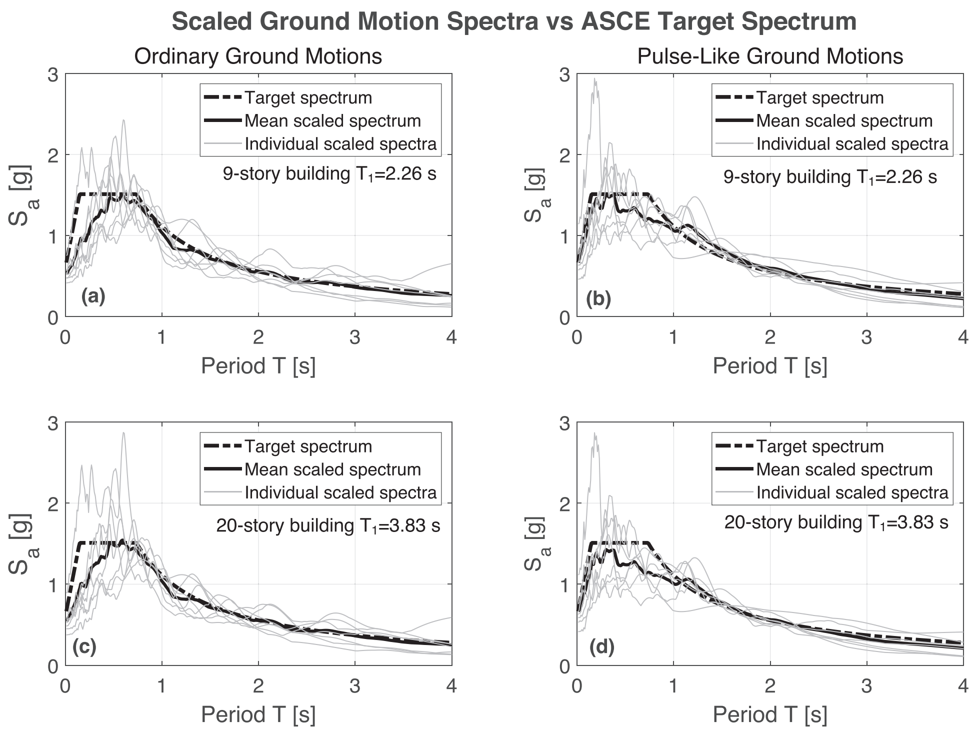

FIGURE 8 | Comparison of scaled ground-motion spectra with the ASCE 7-22 DBE target spectrum for the 9-story (T_1 = 2.26 s) and 20-story (T_1 = 3.83 s) frames. Gray curves show individual scaled records, the solid curve is the mean spectrum, and the dashed curve is the DBE target. Ordinary records are shown in (a,c) and pulse-like records in (b,d).

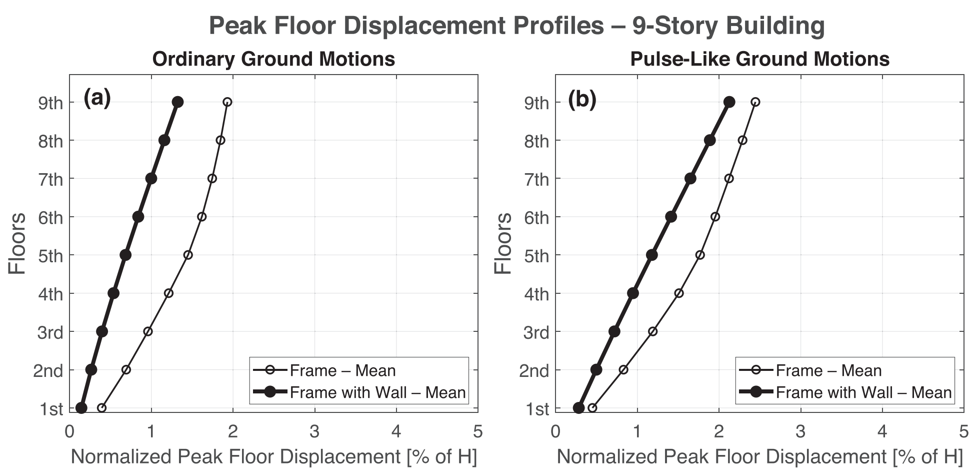

FIGURE 9 | Normalized peak floor displacement profiles for the 9-story frame with and without the rocking wall. (a) Ordinary ground motions; (b) pulse-like ground motions. Curves show mean values across all records; displacements are normalized by the total building height (H).

This redistribution of deformation demand directly mitigates weak-story formation. The magnitude of drift reduction is largest in the stories that exhibit softening behavior in the unretrofitted frame, confirming that the rocking wall not only lowers absolute drift demand but also actively redistributes deformation along the height. This redistribution is a defining characteristic of uplift-dominated systems, which limit plastic curvature accumulation by rotating rather than yielding.

Residual drift profiles are shown in Figure 11. For the bare frame, residual drifts are non-negligible and tend to localize in the same stories where inelastic curvature demands concentrate. Introducing the stepping rocking wall substantially reduces these residual drifts and distributes them more uniformly along the height, consistent with a response governed by uplift and recentering rather than accumulation of plastic deformation within the frame.

Figures 12–14 present the corresponding results for the 20-story frame. The normalized peak floor displacements in Figure 12 show that the taller building is more sensitive to long-period ground-motion content, resulting in larger overall lateral defor-

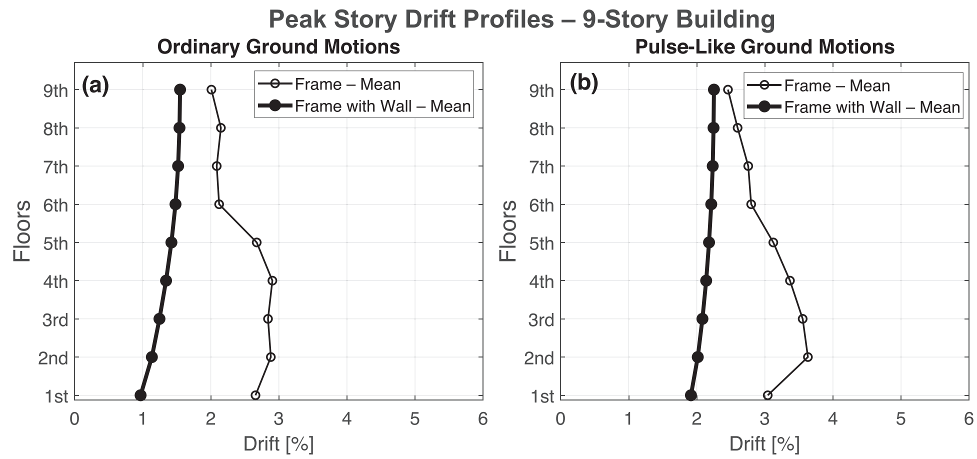

FIGURE 10 | Peak story drift profiles for the 9-story frame with and without the rocking-wall retrofit. (a) Ordinary ground motions; (b) pulse-like ground motions. Mean drift demands across all records are shown.

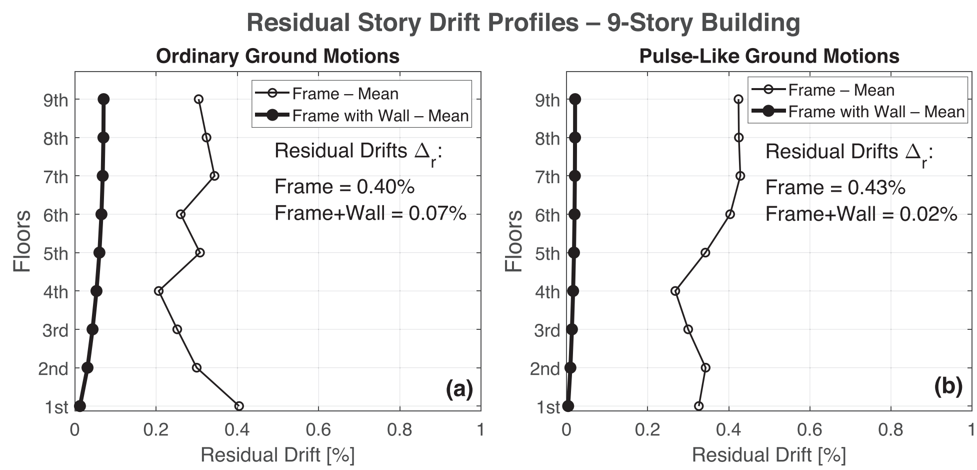

FIGURE 11 | Residual story drift profiles for the 9-story frame with and without the rocking wall. (a) Ordinary ground motions; (b) pulse-like ground motions. Curves show mean residual drift across all records.

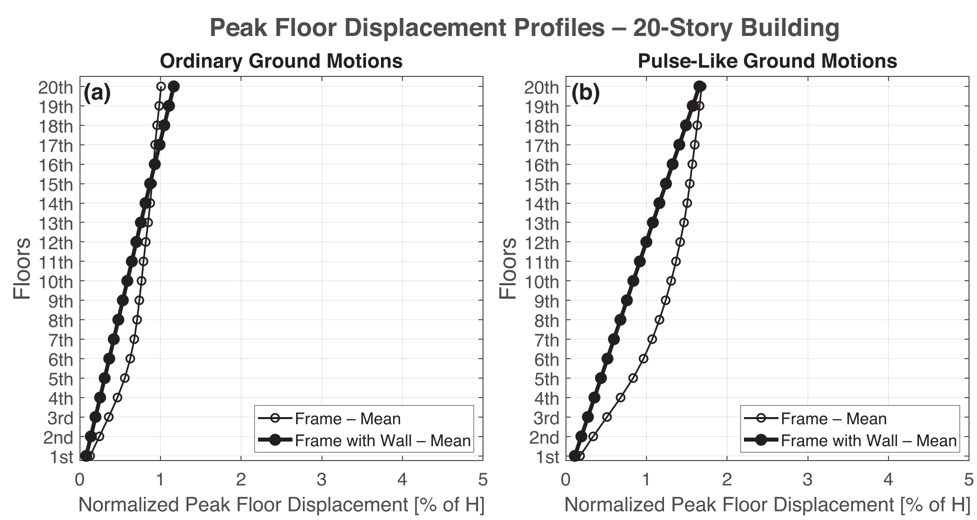

FIGURE 12 | Normalized peak floor displacement profiles for the 20-story frame with and without the rocking wall. (a) Ordinary ground motions; (b) pulse-like ground motions. Curves show mean values across all records; displacements are normalized by the total building height (H).

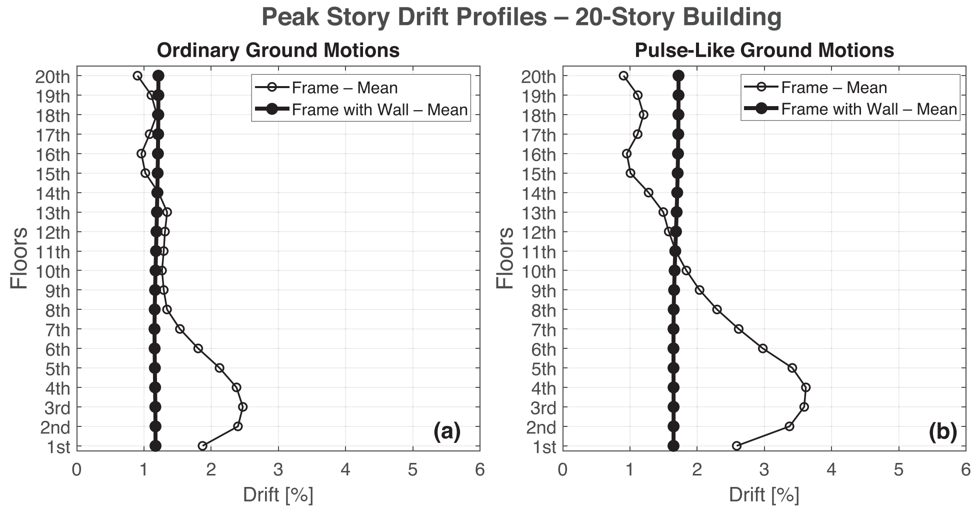

FIGURE 13 | Peak story drift profiles for the 20-story frame with and without the rocking-wall retrofit. (a) Ordinary ground motions; (b) pulse-like ground motions. Mean drift demands across all records are shown.

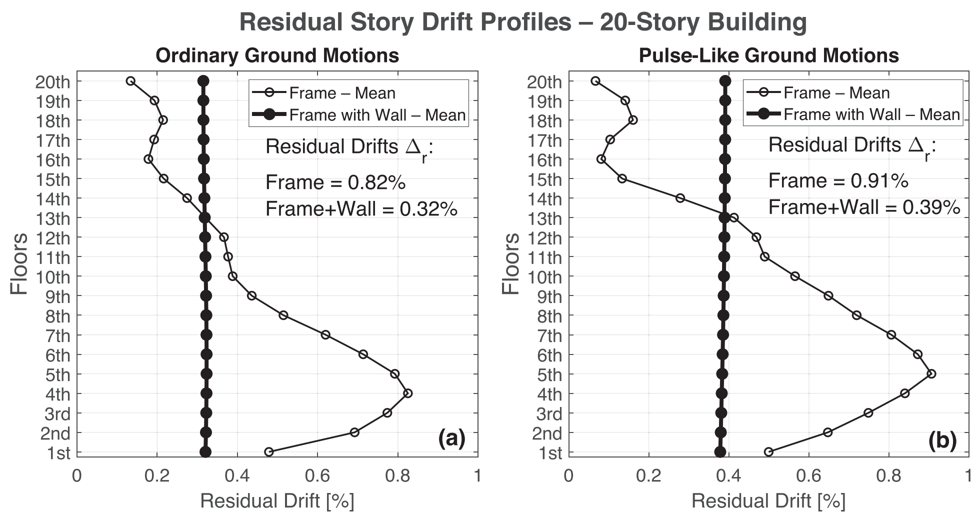

FIGURE 14 | Residual story drift profiles for the 20-story frame with and without the rocking wall. (a) Ordinary ground motions; (b) pulse-like ground motions. Curves show mean residual drift across all records.

mations. Nevertheless, the stepping rocking wall again promotes a first-mode-like profile and reduces roof displacements under both ordinary and pulse-like motions.

Peak drift profiles in Figure 13 reveal a pronounced concentration of drift in the lower stories of the bare frame, especially under pulse-like motions, reflecting a weak-story mechanism. The stepping rocking wall flattens the drift distribution and reduces peak drifts in these critical lower stories, again promoting a first-mode-dominated response.

Residual drifts for the 20-story frame, shown in Figure 14, are larger than those of the 9-story structure, as expected for a more flexible system. For the bare frame, several stories exhibit significant residual deformation, suggesting a non-trivial probability of residual damage. With the stepping rocking wall, residual drifts are consistently reduced, particularly in the lower stories where weak-story behavior is most critical, although non-zero residual deformations remain for this taller building.

Local effects within the wall, including inter-story shear deformation, cracking, and localized damage at the wall toes, are not explicitly modeled in the present formulation. These mechanisms may influence the response of slender rocking walls under large deformation demands and are not captured in the current approach.

4.1 | Residual Drift and Repairability Based on FEMA P-58

Residual drift is a key decision variable in performance-based assessment because it correlates strongly with repairability, expected downtime, and the likelihood of demolition after major earthquakes. FEMA P-58 classifies residual story drift into discrete damage states (DS), summarized in Table 2, with thresholds that distinguish negligible damage (DS0) from minor (DS1), moderate (DS2), severe (DS3), and essentially irreparable damage (DS4). Residual drift is interpreted here as an indicator

TABLE 2 | Damage states for residual story drift ratio (FEMA P-58 [72], Vol. 1, Table C-1).

Damage state	Residual story drift (%)	Description
DS0	$\Delta_{res} < 0.2\%$	Negligible residual drift; fully functional.
DS1	$0.2\% \leq \Delta_{res} < 0.5\%$	Minor residual drift; repairable with limited intervention.
DS2	$0.5\% \leq \Delta_{res} < 1.0\%$	Moderate residual drift; significant repairs required.
DS3	$1.0\% \leq \Delta_{res} < 2.0\%$	Severe residual drift; repair feasibility uncertain.
DS4	$\Delta_{res} \geq 2.0\%$	Extensive damage; building likely irreparable.

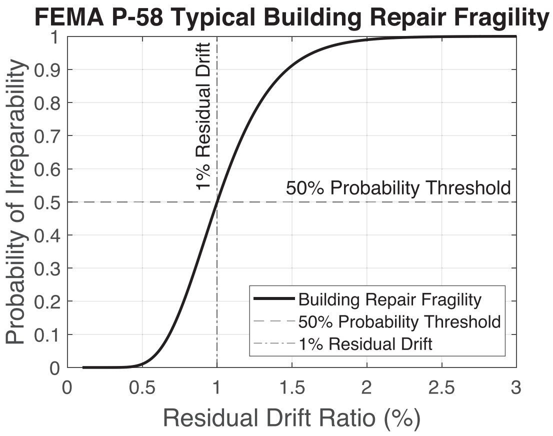

FIGURE 15 | Typical building repair fragility curve as a function of residual drift ratio based on FEMA P-58.

of repairability based on FEMA P-58 criteria. A full performance-based assessment of downtime and economic consequences is not included and would require a more comprehensive PBEE framework.

The repair fragility curve from FEMA P-58 (Figure 15) provides a probabilistic link between residual drift and the likelihood that a building is repairable. At residual drifts below approximately 0.5%, the probability of repair remains high. Beyond 1%, the probability of irreparable damage increases rapidly, reflecting the technical and economic difficulty of restoring frames with large permanent deformations.

The simulated residual drift profiles in Figures 11 and 14 can be interpreted directly using these thresholds. Stories with residual drift exceeding 0.5% fall into DS2 or higher, indicating moderate to severe residual deformation and substantial repair requirements. Stories with residual drift below 0.2% remain in DS0, corresponding to negligible permanent deformation. As shown later in this section, the stepping rocking wall shifts a significant portion of the building height toward lower residual drift ratios, thereby reducing the occurrence of FEMA P-58 damage states associated with costly or infeasible repairs.

4.2 | Weak-Story Quantification via DCF

The response-history results presented above show that the stepping rocking wall alters the distribution of story drift demands in both buildings. While peak story drift is commonly used as a primary response measure, it does not provide information about how deformation is distributed along the height of the structure. As a result, systems with similar peak drift values may exhibit fundamentally different damage patterns depending on whether deformation is distributed or concentrated in a limited number of stories.

To quantify this effect, a DCF is introduced as a scalar measure of drift localization for each ground motion [13, 73]. For a given record k, the DCF is defined as

$$\mathrm{DCF}^{(k)} = \frac{\max_i \Delta_i^{(k)}}{\frac{1}{N_{\mathrm{story}}} \sum_{i=1}^{N_{\mathrm{story}}} \Delta_i^{(k)}}, \tag{7}$$

where $\Delta_i^{(k)}$ is the peak story drift ratio in story i.

Although several prior studies [73, 74] characterize global deformation using the roof-drift ratio $\theta_{\mathrm{roof}} = u_{\mathrm{roof}}/H$, this measure is most appropriate when the drift profile is dominated by the first mode. However, it becomes less reliable when significant drift localization develops.

In the present study, the DCF is defined by normalizing the peak story drift by the mean (height-averaged) drift demand over all stories, providing a direct measure of deformation localization in systems exhibiting soft-story mechanisms or highly nonlinear drift profiles. Values near unity correspond to a uniform, first-mode-dominated deformation pattern, while larger values indicate increasing drift localization and a higher likelihood of weak-story formation.

Table 3 summarizes the mean DCF values. For the 9-story frame, the bare system exhibits a mean DCF of 1.29 for both ordinary and pulse-like motions, indicating moderate drift concentration. With the stepping rocking wall, the mean DCF decreases to 1.10 and 1.06, an 18%–22% reduction that reflects a nearly uniform drift distribution, consistent with the first-mode behavior observed in the drift profiles.

The 20-story frame shows substantially stronger drift localization in its bare configuration: mean DCF values of 1.65 (ordinary motions) and 1.69 (pulse-like motions) indicate that the peak-story drift is approximately 65%–70% larger than the building-average drift. This is typical of weak-story behavior in tall, flexible MRF systems. When the rocking wall is added, the DCF decreases to 1.03 and 1.04, corresponding to a 35%–40% reduction and indicating a restored first-mode shape with minimal drift concentration even under severe pulse-like excitations.

TABLE 3 | Mean drift concentration factor (DCF) for the 9-story and 20-story SAC frames, with and without the stepping rocking-wall retrofit.

		Mean DCF	
Building	**System**	**Ordinary GMs**	**Pulse-like GMs**
9-story	Frame only	1.29	1.29
	Frame with rocking wall	1.10	1.06
20-story	Frame only	1.65	1.69
	Frame with rocking wall	1.03	1.04

Note: Values near unity correspond to uniform, first-mode-dominated deformation patterns. Abbreviation: GM, Ground Motion.

Overall, the DCF results confirm that the stepping rocking wall effectively suppresses drift localization in both buildings, with particularly significant benefits in the 20-story frame, where weak-story formation is more severe. These trends reflect the characteristic behavior of recentering structural systems, in which deformation is redistributed along the height rather than concentrating in a single story.

The response observed in the present study is consistent with behavior reported for recentering structural systems that have been implemented in retrofit applications. For example, the redevelopment of the 680 Folsom Street building in San Francisco, CA introduced a base-isolated core within an existing multi-story steel frame, resulting in engagement of multiple stories and a more uniform drift distribution along the height. In addition, pinned rocking wall systems investigated by Wada et al. [36, 37] have been implemented in existing multi-story steel frames and have demonstrated the feasibility of controlled uplift and recentering at the structural level. While these systems differ in implementation from the present study, they illustrate the broader concept that activating global mechanisms can redistribute deformation demands and reduce weak-story concentration.

In this context, the reduction in DCFs observed in the present study provides a direct quantitative measure of how the rocking mechanism redistributes deformation demands and mitigates weak-story behavior.

4.3 | Residual Drift Distributions in FEMA P-58 Damage States

Residual story drift is a key determinant of post-earthquake repairability within the FEMA P-58 framework. Even when peak drift demands remain moderate, residual deformations can render a building economically or functionally irreparable. For each story and ground motion, residual drift ratios are therefore classified into the FEMA P-58 damage states DS0-DS4 using the thresholds in Table 2. Table 4 summarizes the resulting distributions for both buildings in terms of the fraction of all story-record combinations that fall in each damage state.

In the 9-story bare frame, 22% (ordinary) and 27% (pulse-like) of story-record combinations fall in DS2 ($\Delta_{res} \geq 0.5\%$), indicating non-negligible residual drift demands despite the modest height of the building. No DS3 or DS4 cases are observed. When retrofitted with the stepping rocking wall, all residual drift values fall within DS0 for both ground-motion sets, eliminating residual deformation above 0.2% and indicating complete recentering of the system. For low-rise structures, the rocking wall therefore provides full suppression of residual-drift effects.

The 20-story bare frame displays a markedly different pattern. Under ordinary ground motions, 22% of story-record combinations lie within DS2–DS4, including 3.6% in DS4, a state associated with irreparable damage. Pulse-like motions further amplify these effects, increasing the DS2–DS4 fraction to 30% and producing 4.3% DS4 occurrences. These results highlight the increased vulnerability of tall MRFs to residual-drift accumulation, particularly under near-fault excitation.

The stepping rocking wall substantially modifies this distribution. Under ordinary motions, DS2 and DS4 are eliminated entirely, and the DS2–DS4 fraction decreases from 22% (bare frame) to 14%. Under pulse-like motions, the retrofit fully removes DS4 and maintains a DS3 fraction comparable to that of the bare frame (14.3% vs. 15.0%). The DS2 fraction for the retrofitted frame (0.286) is higher than that of the bare frame (0.150) under pulse-like motions.

This increase in DS2 reflects the spatial redistribution of residual drift rather than an increase in overall damage. In the bare frame, residual deformations concentrate in a small number of stories at DS3–DS4 levels, while adjacent stories remain in DS0. The rocking wall promotes a more uniform residual drift distribution along the height, reducing peak residual demands in critical stories while shifting some previously undamaged stories into DS2.

At the building level, this corresponds to improved repairability: irreparable DS4 outcomes are eliminated, and the proportion of severe damage states is reduced. Interpretation of grouped DS2–DS4 fractions should therefore be made with care. DS2 corresponds to repairable damage, whereas DS3–DS4 may be associated with replacement. A full performance-based assessment would be required to quantify these distinctions.

Taken together, the residual-drift classifications for both buildings demonstrate that the stepping rocking wall eliminates the most damaging irreparable states (DS4), suppresses weak-story residual-drift accumulation, and shifts the overall distribution toward more favorable repairability classes. These improvements persist across ordinary and pulse-like ground motions and are particularly impactful in the taller 20-story frame.

Figure 16 provides a compact visualization of these distributions. Each stacked bar shows the fraction of all story-record responses that fall in each FEMA P-58 residual-drift damage state for a given building and retrofit configuration. The results are plotted separately for ordinary and pulse-like motions. The figure highlights the elimination of DS2–DS4 in the 9-story retrofitted frame and the removal of DS4 in the 20-story retrofitted frame, and illustrates how the retrofit shifts the distribution from higher to lower damage states.

TABLE 4 | Distribution of FEMA P-58 residual-drift damage states (DS0-DS4) for the 9-story and 20-story SAC frames, with and without the stepping rocking-wall retrofit.

Building	System	DS0	DS1	DS2	DS3	DS4
9-story	Frame only (ordinary GMs)	0.397	0.381	0.222	0.000	0.000
	Frame only (pulse-like GMs)	0.238	0.492	0.270	0.000	0.000
	Frame with rocking wall (ordinary GMs)	1.000	0.000	0.000	0.000	0.000
	Frame with rocking wall (pulse-like GMs)	1.000	0.000	0.000	0.000	0.000
20-story	Frame only (ordinary GMs)	0.379	0.393	0.164	0.029	0.036
	Frame only (pulse-like GMs)	0.450	0.250	0.150	0.107	0.043
	Frame with rocking wall (ordinary GMs)	0.471	0.386	0.029	0.114	0.000
	Frame with rocking wall (pulse-like GMs)	0.571	0.000	0.286	0.143	0.000

Note: Values denote fractions of story-record combinations.

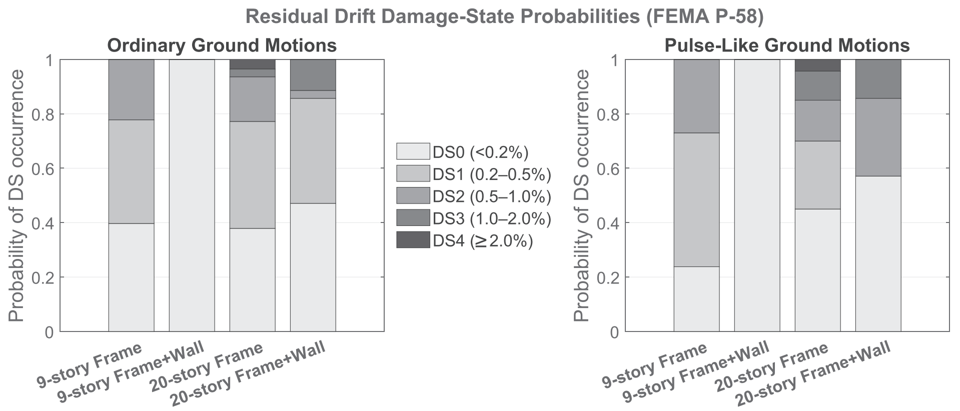

FIGURE 16 | Residual-drift damage-state probabilities (FEMA P-58) for the 9-story and 20-story frames with and without the stepping rocking-wall retrofit. Left: ordinary ground motions; right: pulse-like ground motions. Bars show the fraction of story-record combinations in each residual-drift damage state (DS0–DS4).

Overall, the recorded-motion results show that the stepping rocking wall systematically reshapes the seismic response of both SAC frames. In both the 9-story and 20-story buildings, the retrofit enforces a first-mode-dominated deformation pattern, reduces peak story drifts in the most highly demanded stories, and suppresses weak-story drift localization as quantified by the DCF. At the same time, residual drifts are substantially reduced, shifting story-level performance toward lower FEMA P-58 damage states: the 9-story retrofitted frame exhibits negligible residual deformation (DS0 throughout), while the 20-story retrofitted frame eliminates irreparable DS4 outcomes and significantly curtails severe residual drift demands. These trends hold under both ordinary and pulse-like excitations, although the taller frame remains more sensitive to the period and intensity of near-fault velocity pulses, motivating the spectral pulse-based investigation in the next section.

5 | Drift Spectra Under Mathematical Pulses

The recorded-motion results in Section 4 showed that long-period velocity pulses can drive substantial story drifts and trigger weak-story mechanisms in steel MRFs. While recorded pulse-like motions provide valuable insight, they do not span the full range of pulse periods and amplitudes that govern structural response. To systematically evaluate how pulse characteristics influence drift demands, this section develops transient drift spectra using idealized mathematical wavelets whose amplitude and pulse period serve as independent control parameters. This approach isolates the effects of pulse severity and time scale and complements the broader response obtained from recorded ground motions. Wavelet analysis provides a means of extracting and parameterizing the dominant impulsive component of near-fault records. Following the formulation introduced by Vassiliou & Makris [75], two analytical pulses are employed: (i) the Symmetric Ricker Wavelet, corresponding to the second derivative of a Gaussian function, and (ii) the Antisymmetric Ricker Wavelet, corresponding to the third derivative of a Gaussian function (both shown in Figure 17). These wavelets capture the key attributes of near-fault pulses, including amplitude, duration, and polarity, while preserving the features known to correlate with large structural demands. Figure 17 shows representative examples of matched pulses for several well-known near-fault ground motions [75–78].

The Symmetric Ricker Wavelet adopted in this study is defined as

$$\ddot{u}_g(t) = a_p \left(1 - \frac{2\pi^2 t^2}{T_p^2}\right) e^{-\frac{1}{2}\frac{2\pi^2 t^2}{T_p^2}}, \tag{8}$$

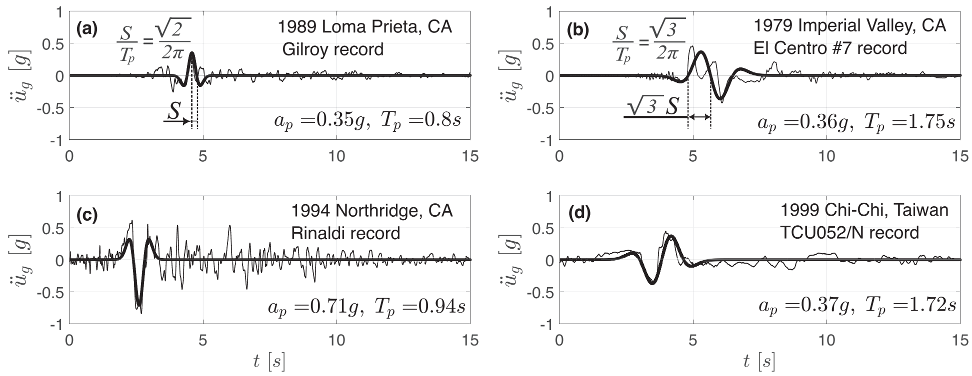

FIGURE 17 | Matching of acceleration records with a symmetric Ricker wavelet (a,c) and an antisymmetric Ricker wavelet (b,d). Earthquake time-histories: (a) Gilroy record from the 1989 Loma Prieta, California, (b) El Centro array 7 of the 1979 Imperial Valley, California, (c) Rinaldi record from the 1994 Northridge, California, and (d) TCU052/N record from the 1999 Chi-Chi Taiwan.

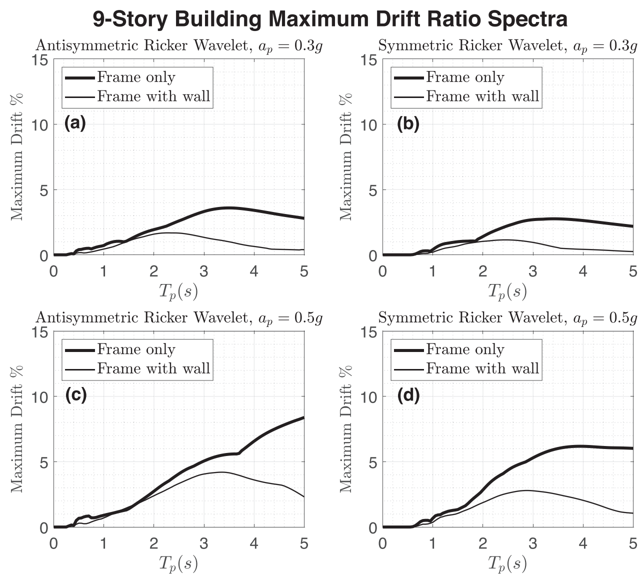

FIGURE 18 | Transient drift ratio spectra for the 9-story building with and without a rocking wall. (a,c) Antisymmetric Ricker pulses with $a_p = 0.3$ and 0.5g; (b,d) Symmetric Ricker pulses.

where T_p is the pulse period and a_p is the peak pulse acceleration. The Antisymmetric Ricker Wavelet is expressed as

$$\ddot{u}_g(t) = \frac{a_p}{\beta}\left(\frac{4\pi^2 t^2}{3T_p^2} - 3\right)\frac{2\pi t}{\sqrt{3}T_p}e^{-\frac{1}{2}\frac{4\pi^2 t^2}{3T_p^2}}, \tag{9}$$

with $\beta = 1.38$ ensuring that the peak acceleration equals a_p. These wavelets are illustrated in Figure 17.

Figure 18 presents the resulting transient drift spectra for the 9-story building subjected to symmetric and antisymmetric Ricker pulses with amplitudes $a_p = 0.3$ and 0.5g. The horizontal axis shows the pulse period T_p, varied from 0 to 5 s. In each plot, the thick line denotes the peak story drift ratio of the bare MRF, and the thin line corresponds to the frame retrofitted with a stepping rocking wall.

Across all pulse periods and amplitudes, the rocking wall consistently reduces peak drift demands. This reduction becomes especially pronounced when the pulse period approaches or exceeds the first-mode period of the structure ($T_1 \approx 2.26$ s), where long-period pulses impart a quasi-static displacement impulse that produces large drifts in the unretrofitted MRF. The rocking wall mitigates this effect by permitting uplift and rotation, thereby limiting permanent deformation in the frame and reducing the likelihood of exceeding FEMA P-58 repairability thresholds [72].

The observed increase in response with increasing pulse amplitude reflects nonlinear amplification associated with rocking-induced uplift and period-dependent interaction between the input pulse and the structural system. For longer-period systems, increased excitation amplitude leads to larger uplift demands and prolonged rocking phases, which in turn amplify displacement response. This effect is less pronounced in the frame-only system due to the absence of uplift-driven stiffness redistribution and recentering behavior.

Figure 19 shows the corresponding drift spectra for the 20-story building. Due to its greater flexibility ($T_1 \approx 3.83$ s), this structure experiences stronger amplification of drift demands under long-period pulses. Nevertheless, the rocking wall again substantially reduces these demands, particularly for pulse periods near or above the first-mode period. Antisymmetric pulses produce slightly larger drift demands than symmetric pulses of the same a_p and T_p, reflecting their stronger low-frequency velocity content and greater capacity to induce residual deformation in flexible frames.

For both buildings, the drift spectra demonstrate that rocking walls are particularly effective in mitigating the damaging effects of long-period pulses that align with the structural period range. By reducing both peak and residual drift demands across a wide range of T_p–a_p combinations, the stepping rocking wall improves repairability and reduces the probability of drift-governed performance losses as defined in FEMA P-58.

6 | Response Under Increased Shaking Intensity

The transient drift spectra presented in Section 5 showed that long-period pulse-like excitations can substantially amplify drift demands, particularly when the pulse period approaches the

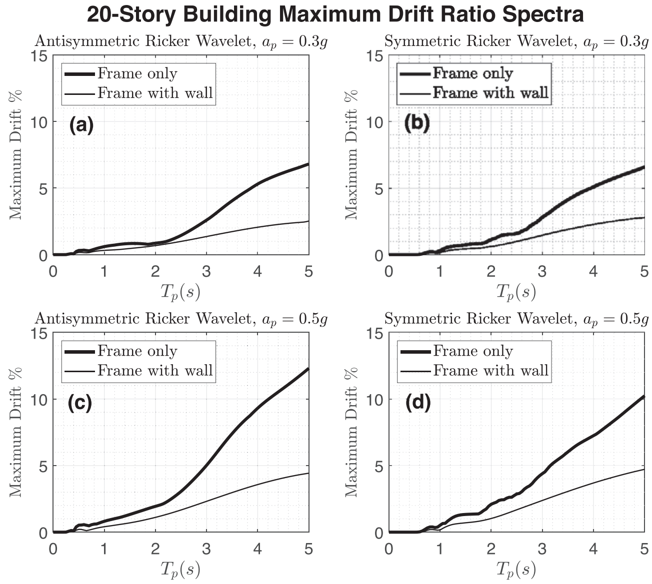

FIGURE 19 | Transient drift ratio spectra for the 20-story building with and without a rocking wall. (a,c) Antisymmetric Ricker pulses with $a_p = 0.3$ and 0.5g; (b,d) Symmetric Ricker pulses.

fundamental period of the structure. These observations motivate an additional investigation to determine whether the beneficial trends observed at the DBE level, including reduced peak drift, reduced residual drift, and suppression of drift concentration, persist under stronger shaking. To address this question, an additional set of nonlinear response-history analyses was performed using the pulse-like ground motions scaled to the MCE hazard level.

The objective of this section is to evaluate whether the principal conclusions regarding drift redistribution and residual-drift reduction remain valid when the excitation intensity is increased beyond the DBE level. This supplemental analysis directly addresses the question of whether the beneficial effects of the stepping rocking wall are preserved under more severe near-fault shaking.

Figure 20 compares the mean peak story drift profiles of the 9-story and 20-story buildings under the MCE-scaled pulse-like records. In both structures, the unretrofitted frames continue to exhibit pronounced drift localization, with deformation concentrated in a limited number of lower stories. This concentration is particularly evident in the 20-story frame, where the drift profile is characteristic of a weak-story mechanism. In contrast, the stepping rocking wall maintains a substantially more uniform drift distribution along the height, consistent with the first-mode-dominated response observed at the DBE level.

Table 5 summarizes three scalar response measures: the median maximum peak interstory drift ratio (PIDR), the median maximum residual interstory drift ratio (RIDR), and the median DCF. These metrics confirm that the retrofit remains effective under increased shaking intensity.

For the 9-story building, the median maximum PIDR decreases from 6.03% in the bare frame to 3.42% with the rocking wall, corresponding to a reduction of approximately 43%. The median maximum RIDR decreases from 0.92% to 0.05%, representing a reduction of approximately 95%. The median DCF decreases from 1.32 to 1.04, indicating that the retrofit largely eliminates drift localization and promotes a more uniformly distributed deformation pattern.

For the 20-story building, the median maximum PIDR decreases from 3.74% to 1.63%, corresponding to a reduction of approximately 56%. The median maximum RIDR decreases from 1.56% to 0.45%, representing a reduction of approximately 71%. The median DCF decreases from 1.91 to 1.03, indicating a substantial suppression of weak-story behavior and a return to a nearly first-mode-shaped response.

The residual drift reductions are particularly significant when interpreted in the context of FEMA P-58 repairability criteria. In the unretrofitted systems, the median residual drifts for both buildings exceed the 0.5% threshold associated with moderate to severe repair demands. In the retrofitted systems, residual drifts are reduced below this threshold, indicating a markedly lower likelihood of repair-precluding permanent deformations even under MCE-level excitation.

Overall, the MCE-level analyses demonstrate that the principal findings of this study are not limited to DBE-level shaking. Although absolute drift demands increase as expected, the stepping rocking wall continues to (i) reduce peak interstory drift, (ii) substantially reduce residual deformation, and (iii) suppress drift concentration associated with weak-story mechanisms. These results provide additional evidence that the retrofit remains effective under severe pulse-like ground motions and that the beneficial response trends identified at the DBE level are robust to increased shaking intensity.

7 | Conclusions

This study evaluated the seismic response of 9-story and 20-story SAC Los Angeles moment-resisting steel frames retrofitted with a stepping rocking wall. The analyses showed that the unretrofitted frames are highly sensitive to long-period velocity pulses, which produce concentrated drift demands and significant residual deformations, particularly in the more flexible 20-story building.

Introducing the stepping rocking wall modifies this behavior by enabling uplift and recentering, which alters the effective stiffness and promotes a more uniform, first-mode-dominated response. As a result, peak and residual drift demands are reduced, and the tendency for weak-story formation is mitigated. This effect is quantified using a DCF, which captures deformation localization not reflected in conventional peak drift metrics and consistently indicates reduced drift concentration across both ordinary and pulse-like ground motions.

FEMA P-58-based interpretation of residual drift further indicates a reduction in the likelihood of repair-precluding damage states, suggesting improved repairability. Transient drift spectra constructed using Ricker pulse excitations show that the retrofitted systems are less sensitive to resonance between structural period

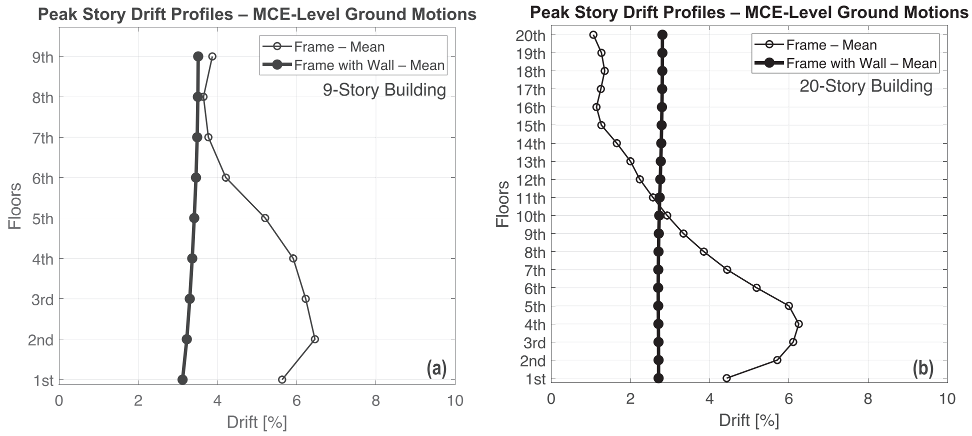

FIGURE 20 | Mean peak story drift profiles under pulse-like ground motions scaled to the maximum considered earthquake (MCE) level for the (a) 9-story and (b) 20-story SAC frames, with and without the stepping rocking-wall retrofit.

TABLE 5 | Summary of MCE-level response metrics for the 9-story and 20-story SAC frames under pulse-like ground motions, with and without the stepping rocking-wall retrofit.

Building	System	Median max. PIDR (%)	Median max. RIDR (%)	Median DCF
9-story	Frame only	6.03	0.92	1.32
	Frame with rocking wall	3.42	0.05	1.04
20-story	Frame only	3.74	1.56	1.91
	Frame with rocking wall	1.63	0.45	1.03

Abbreviations: PIDR, peak interstory drift ratio; RIDR, residual interstory drift ratio; DCF, drift concentration factor.

and pulse period, a primary driver of drift amplification in flexible frames.

Additional analyses using pulse-like ground motions scaled to the MCE level indicate that the principal response trends identified at the DBE level persist under stronger shaking. In both buildings, the retrofit continues to reduce peak interstory drift, substantially reduce residual drift, and suppress drift concentration, with median DCF values approaching unity.

Overall, the results demonstrate that stepping rocking wall retrofits can effectively reduce drift concentration and residual deformation in MRFs subjected to long-period ground motions.

The results also indicate that these systems are particularly effective in mid- to high-rise frames, where drift localization and residual deformation govern performance. By promoting a more distributed deformation pattern and limiting weak-story formation, the retrofit reduces the likelihood of severe damage without relying on increased stiffness or strength.

This study establishes the system-level mechanical basis for stepping rocking wall retrofits and highlights their potential to improve deformation distribution and repairability. Further investigation is needed to address implementation aspects, including diaphragm force demands, foundation design, and constructability considerations.

Data Availability Statement

The data that support the findings of this study are available from the corresponding author upon reasonable request.

References

1. V. V. Bertero, S. A. Mahin, and R. A. Herrera, "Aseismic Design Implications of Near-Fault San Fernando Earthquake Records," *Earthquake Engineering & Structural Dynamics* 6, no. 1 (1978): 31–42, https://doi.org/10.1002/eqe.4290060105.

2. B. A. Bolt, "The San Fernando Valley, California, Earthquake of February 9 1971: Data on Seismic Hazards," *Bulletin of the Seismological Society of America* 61, no. 2 (1971): 501–510.

3. B. A. Bolt, "The San Fernando Earthquake, 1971. Magnitudes, Aftershocks, and Fault Dynamics," *Bulletin 196, California Division of Mines and Geology* (1975).

4. N. Makris and C. J. Black, "Evaluation of Peak Ground Velocity as a "Good" Intensity Measure for Near-Source Ground Motions," *Journal of Engineering Mechanics* 130, no. 9 (2004): 1032–1044, https://doi.org/10.1061/(ASCE)0733-9399(2004)130:9(1032).

5. T. Paulay, "The Coupling of Reinforced Concrete Shear Walls," in *The Fourth World Conference on Earthquake Engineering, Santiago, Chile* (1969), Conference Proceedings.

6. M. Fintel, "Ductile Shear Walls in Earthquake-Resistant Multistory Buildings," in *Wind and Seismic Effects: Proceedings of the Seventh Joint Panel Conference of the US-Japan Cooperative Program in Natural Resources, Tokyo, Japan*, vol. 470 (US Department of Commerce, National Bureau of Standards, 1975), Conference Proceedings, p. 33.

7. K. Emori and W. C. Schnobrich, *Analysis of Reinforced Concrete Frame-Wall Structures for Strong Motion Earthquakes* (Report no. SRS-457, University of Illinois at Urbana-Champaign, 1978. http://hdl.handle.net/2142/13919, 1978).

8. V. V. Bertero, "Seismic Behavior of R/C Wall Structural Systems," in *The 7th World Conference on Earthquake Engineering, Istanbul, Turkey* (1969), Conference Proceedings, 323–330.

9. A. E. Aktan and V. V. Bertero, "Seismic Response of R/C Frame-Wall Structures," *Journal of Structural Engineering* 110 (1984): 1803–1821, https://doi.org/10.1061/(ASCE)0733-9445(1984)110:8(1803).

10. U.S. Geological Survey (USGS), "USGS Photographic Library," ID aeq00019, https://library.usgs.gov/photo/. [access date: 01-21-2024] (1964).

11. NOAA Natural Hazard Images Database, "Event: January 1995 Hanshin-Awaji (Kobe), Japan Images, NOAA National Centers for Environmental Information, https://doi.org/10.7289/v5154f01. [access date: 05-10-2024]," (2012).

12. J. McCormick, H. Aburano, M. Ikenaga, and M. Nakashima, "Permissible Residual Deformation Levels for Building Structures Considering Both Safety and Human Elements," in *The 14th World Conference on Earthquake Engineering, Beijing, China* (2008), Conference Proceedings, pp. 12–17.

13. J. Erochko, C. Christopoulos, R. Tremblay, and H. Choi, "Residual Drift Response of SMRFS and BRB Frames in Steel Buildings Designed According to ASCE 7-05," *Journal of Structural Engineering* 137, no. 5 (2011): 589–599, https://doi.org/10.1061/(ASCE)ST.1943-541X.0000296.

14. M. Bruneau and G. MacRae, "Building Structural Systems in Christchurch's Post-Earthquake Reconstruction," *Earthquake Spectra* 35 (2019): 1953–1978, https://doi.org/10.1193/052818EQS126O.

15. J. Worley and P. Quenneville, "Residual Drift–the Ignored Outcome," https://www.structuremag.org/article/residual-drift-the-ignored-outcome/.

16. American Society of Civil Engineers, *Minimum Design Loads and Associated Criteria for Buildings and Other Structures (ASCE/SEI 7-22)* (American Society of Civil Engineers, 2022), https://doi.org/10.1061/9780784415788.

17. American Society of Civil Engineers, *Seismic Evaluation and Retrofit of Existing Buildings (ASCE/SEI 41-23)* (American Society of Civil Engineers, 2023), https://doi.org/10.1061/9780784416112.

18. G. W. Housner, "The Behavior of Inverted Pendulum Structures During Earthquakes," *Bulletin of the Seismological Society of America* 53, no. 2 (1963): 403–417, https://doi.org/10.1785/BSSA0530020403.

19. J. M. Kelly, R. Skinner, and A. Heine, "Mechanisms of Energy Absorption in Special Devices for Use in Earthquake Resistant Structures," *Bulletin of the New Zealand National Society for Earthquake Engineering* 5, no. 3 (1972): 63–88, https://doi.org/10.5459/bnzsee.5.3.63-88.

20. R. Skinner, J. Kelly, and A. Heine, "Hysteretic Dampers for Earthquake-Resistant Structures," *Earthquake Engineering & Structural Dynamics* 3, no. 3 (1974): 287–296, https://doi.org/10.1002/eqe.4290030307.

21. J. Meek, "Dynamic Response of Tipping Core Buildings," *Earthquake Engineering & Structural Dynamics* 6, no. 5 (1978): 437–454, https://doi.org/10.1002/eqe.4290060503.

22. M. N. Priestley, "Overview of Presss Research Program," *PCI Journal* 36 (1991): 50–57, https://doi.org/10.15554/pcij.07011991.50.57.

23. M. N. Priestley, "The Presss Program Current Status and Proposed Plans for Phase III," *PCI Journal* 41, no. 2 (1996): 22–40, https://doi.org/10.15554/pcij.03011996.22.40.

24. S. D. Nakaki, J. F. Stanton, and S. Sritharan, "An Overview of the Presss Five-Story Precast Test Building," *PCI Journal* 44, no. 2 (1999): 26–39, https://doi.org/10.15554/pcij.03011999.26.39.

25. M. N. Priestley, S. Sritharan, J. R. Conley, and S. Pampanin, "Preliminary Results and Conclusions From the Presss Five-Story Precast Concrete Test Building," *PCI Journal* 44, no. 6 (1999): 42–67, https://doi.org/10.15554/pcij.11011999.42.67.

26. Y. C. Kurama, R. Sause, S. Pessiki, and L.-W. Lu, "Lateral Load Behavior and Seismic Design of Unbonded Post-Tensioned Precast Concrete Walls," *Structural Journal* 96 (1999): 622–632, https://doi.org/10.14359/700.

27. Y. C. Kurama, R. Sause, S. Pessiki, and L.-W. Lu, "Seismic Response Evaluation of Unbonded Post-Tensioned Precast Walls," *Structural Journal* 99, no. 5 (2002): 641–651, https://doi.org/10.14359/12304.

28. T. Holden, J. Restrepo, and J. B. Mander, "Seismic Performance of Precast Reinforced and Prestressed Concrete Walls," *Journal of Structural Engineering* 129 (2003): 286–296, https://doi.org/10.1061/(ASCE)0733-9445(2003)129:3(286).

29. J. B. Mander and C.-T. Cheng, "Seismic Resistance of Bridge Piers Based on Damage Avoidance Design," *Technical Report NCEER-97-0014, National Center for Earthquake Engineering Research, University at Buffalo, State University of New York* (1997).

30. J. J. Ajrab, G. Pekcan, and J. B. Mander, "Rocking Wall–Frame Structures With Supplemental Tendon Systems," *Journal of Structural Engineering* 130, no. 6 (2004): 895–903, https://doi.org/10.1061/(ASCE)0733-9445(2004)130:6(895).

31. B. Alavi and H. Krawinkler, "Strengthening of Moment-Resisting Frame Structures Against Near-Fault Ground Motion Effects," *Earthquake Engineering & Structural Dynamics* 33 (2004): 707–722, https://doi.org/10.1002/eqe.370.

32. A. Filiatrault, J. Restrepo, and C. Christopoulos, "Development of Self-Centering Earthquake Resisting Systems," in *13th World Conference on Earthquake Engineering* (2004), Conference Proceedings, pp. 1–6.

33. J. I. Restrepo and A. Rahman, "Seismic Performance of Self-Centering Structural Walls Incorporating Energy Dissipators," *Journal of Structural Engineering* 133 (2007): 1560–1570, https://doi.org/10.1061/(ASCE)0733-9445(2007)133:11(1560).

34. B. Erkmen and A. E. Schultz, "Self-Centering Behavior of Unbonded, Post-Tensioned Precast Concrete Shear Walls," *Journal of Earthquake Engineering* 13 (2009): 1047–1064, https://doi.org/10.1080/13632460902859136.

35. L. Toranzo, J. Restrepo, J. Mander, and A. Carr, "Shake-Table Tests of Confined-Masonry Rocking Walls With Supplementary Hysteretic Damping," *Journal of Earthquake Engineering* 13, no. 6 (2009): 882–898.

36. A. Wada, Z. Qu, S. Motoyui, and H. Sakata, "Seismic Retrofit of Existing SRC Frames Using Rocking Walls and Steel Dampers," *Frontiers of Architecture and Civil Engineering in China* 5 (2011): 259–266.

37. Z. Qu, A. Wada, S. Motoyui, H. Sakata, and S. Kishiki, "Pin-Supported Walls for Enhancing the Seismic Performance of Building Structures," *Earthquake Engineering & Structural Dynamics* 41, no. 14 (2012): 2075–2091.

38. N. Makris and M. Aghagholizadeh, "The Dynamics of an Elastic Structure Coupled With a Rocking Wall," *Earthquake Engineering & Structural Dynamics* 46, no. 6 (2017): 945–962, https://doi.org/10.1002/eqe.2838.

39. M. Aghagholizadeh and N. Makris, "Seismic Response of a Yielding Structure Coupled With a Rocking Wall," *Journal of Structural Engineering* 144, no. 2 (2018): 04017196, https://doi.org/10.1061/(ASCE)ST.1943-541X.0001894.

40. M. Aghagholizadeh and N. Makris, "Earthquake Response Analysis of Yielding Structures Coupled With Vertically Restrained Rocking Walls," *Earthquake Engineering & Structural Dynamics* 47, no. 15 (2018): 2965–2984, https://doi.org/10.1002/eqe.3116.

41. N. Makris and M. Aghagholizadeh, "Effect of Supplemental Hysteretic and Viscous Damping on Rocking Response of Free-Standing Columns,"

Journal of Engineering Mechanics 145, no. 5 (2019): 04019028, https://doi.org/10.1061/(ASCE)EM.1943-7889.0001596.

42. M. Aghagholizadeh and N. Makris, "Response Analysis of Yielding Structures Coupled to Rocking Walls With Supplemental Damping," *Earthquake Engineering & Structural Dynamics* 50, no. 10 (2021): 2672–2689, https://doi.org/10.1002/eqe.3466.

43. M. Aghagholizadeh and N. Makris, *Moment Resisting Frames Coupled with Rocking Walls Subjected to Earthquakes*, Peer Report 2022/03 ed (Pacific Earthquake Engineering Research Center, 2022), https://doi.org/10.55461/MXXS2889.

44. A. Nicknam and A. Filiatrault, "Numerical Evaluation of Seismic Response of Buildings Equipped With Propped Rocking Wall Systems," in *10th US National Conference on Earthquake Engineering: Frontiers of Earthquake Engineering* (2014).

45. L. Wiebe and C. Christopoulos, "Performance-Based Seismic Design of Controlled Rocking Steel Braced Frames. I: Methodological Framework and Design of Base Rocking Joint," *Journal of Structural Engineering* 141 (2015): 04014226, https://doi.org/10.1061/(ASCE)ST.1943-541X.0001202.

46. L. Wiebe and C. Christopoulos, "Performance-Based Seismic Design of Controlled Rocking Steel Braced Frames. II: Design of Capacity-Protected Elements," *Journal of Structural Engineering* 141 (2015): 04014227, https://doi.org/10.1061/(ASCE)ST.1943-541X.0001201.

47. C. E. Grigorian and M. Grigorian, "Performance Control and Efficient Design of Rocking-Wall Moment Frames," *Journal of Structural Engineering* 142, no. 2 (2016): 04015139, https://doi.org/10.1061/(ASCE)ST.1943-541X.0001411.

48. M. Nazari, S. Sritharan, and S. Aaleti, "Single Precast Concrete Rocking Walls as Earthquake Force-Resisting Elements," *Earthquake Engineering & Structural Dynamics* 46 (2017): 753–769, https://doi.org/10.1002/eqe.2829.

49. L. Gioiella, A. Balducci, S. Carbonari, F. Gara, and L. Dezi, "An Innovative Seismic Protection System for Existing Buildings: External Dissipative Towers," in *Proceedings of the 16th World Conference on Earthquake Engineering (16WCEE), Santiago, Chile* (2017), 9–13.

50. A. Di Egidio, S. Pagliaro, C. Fabrizio, and A. M. de Leo, "Seismic Performance of Frame Structures Coupled With an External Rocking Wall," *Engineering Structures* 224 (2020): 111207, https://doi.org/10.1016/j.engstruct.2020.111207.

51. A. Di Egidio, S. Pagliaro, and C. Fabrizio, "Combined Use of Rocking Walls and Inerters to Improve the Seismic Response of Frame Structures," *Journal of Engineering Mechanics* 147, no. 5 (2021): 04021016, https://doi.org/10.1061/(ASCE)EM.1943-7889.0001920.

52. C. Zhong and C. Christopoulos, "Shake Table Testing of Shear-Controlling Rocking Isolation Podium System for Mitigating Higher-Mode Effects in Tall Buildings," *Journal of Structural Engineering* 149 (2023): 04023026, https://doi.org/10.1061/JSENDH.STENG-12000.

53. M. Zaki, C. Zhong, and C. Christopoulos, "Analytical Study on the Predictability of Controlled Rocking Frame and Podium Systems," *Earthquake Engineering & Structural Dynamics* 54 (2025): 1558–1578, https://doi.org/10.1002/eqe.4323.

54. S. Pei, J. W. van de Lindt, A. R. Barbosa, et al., "Experimental Seismic Response of a Resilient 2-Story Mass-Timber Building With Post-Tensioned Rocking Walls," *Journal of Structural Engineering* 145, no. 11 (2019): 04019120.

55. S. Pei, K. L. Ryan, J. W. Berman, et al., "Shake-Table Testing of a Full-Scale 10-Story Resilient Mass Timber Building," *Journal of Structural Engineering* 150, no. 12 (2024): 04024183, https://doi.org/10.1061/JSENDH.STENG-13752.

56. D. M. Dowden, A. Tatar, J. W. Berman, and S. Pei, "Shake-Table Test of a Seismically Resilient 10-Story Mass Timber Building With Supplemental Uplift Friction Dampers," *Journal of Structural Engineering* 151, no. 1 (2025): 04024199, https://doi.org/10.1061/JSENDH.STENG-13788.

57. R. Bouc, "Forced Vibrations of Mechanical Systems With Hysteresis," in *Proceedings of the Fourth Conference on Nonlinear Oscillations, 1967* (1967).

58. Y.-K. Wen, "Method for Random Vibration of Hysteretic Systems," *Journal of the Engineering Mechanics Division* 102, no. 2 (1976): 249–263.

59. T. T. Baber and Y.-K. Wen, "Random Vibration of Hysteretic, Degrading Systems," *Journal of the Engineering Mechanics Division* 107, no. 6 (1981): 1069–1087.

60. M. F. Vassiliou and N. Makris, "Dynamics of the Vertically Restrained Rocking Column," *Journal of Engineering Mechanics* 141, no. 12 (2015): 04015049, https://doi.org/10.1061/(ASCE)EM.1943-7889.0000953.

61. N. Makris and M. F. Vassiliou, "Dynamics of the Rocking Frame With Vertical Restrainers," *Journal of Structural Engineering* 141, no. 10 (2015): 04014245, https://doi.org/10.1061/(ASCE)ST.1943-541X.0001231.

62. SAC Joint Venture and Guidelines Development Committee, *Recommended Seismic Design Criteria for New Steel Moment-Frame Buildings* (Federal Emergency Management Agency, 2000).

63. OpenSees, *version 3.7.1* (Pacific Earthquake Engineering Research Center (PEER), University of California, 2025). http://opensees.berkeley.edu/.

64. A. Gupta and H. Krawinkler, *Seismic Demands for Performance Evaluation of Steel Moment Resisting Frame Structures (SAC Task 5.4. 3)* (John A. Blume Earthquake Engineering Center, Stanford University, 1999).

65. A. Gupta and H. Krawinkler, "Behavior of Ductile SMRFS at Various Seismic Hazard Levels," *Journal of Structural Engineering* 126, no. 1 (2000): 98–107, https://doi.org/10.1061/(ASCE)0733-9445(2000)126:1(98).

66. Y. Ohtori, R. Christenson, B. Spencer Jr, and S. Dyke, "Benchmark Control Problems for Seismically Excited Nonlinear Buildings," *Journal of Engineering Mechanics* 130, no. 4 (2004): 366–385, https://doi.org/10.1061/(ASCE)0733-9399(2004)130:4(366).

67. M. F. Vassiliou, K. R. Mackie, and B. Stojadinović, "A Finite Element Model for Seismic Response Analysis of Deformable Rocking Frames," *Earthquake Engineering & Structural Dynamics* 46, no. 3 (2016): 447–466, https://doi.org/10.1002/eqe.2799.

68. M. Aghagholizadeh, "A Finite Element Model for Seismic Response Analysis of Vertically-Damped Rocking-Columns," *Engineering Structures* 219 (2020): 110894, https://doi.org/10.1016/j.engstruct.2020.110894.

69. Pacific Earthquake Engineering Research Center (PEER), "NGA-West2 Ground Motion Database," https://ngawest2.berkeley.edu/site (2025), accessed: 2025-08-07.

70. American Society of Civil Engineers, "ASCE Hazard Tool," https://ascehazardtool.org/ (2022), accessed: 2025-11-07.

71. H. M. Hilber, T. J. Hughes, and R. L. Taylor, "Improved Numerical Dissipation for Time Integration Algorithms in Structural Dynamics," *Earthquake Engineering & Structural Dynamics* 5, no. 3 (1977): 283–292, https://doi.org/10.1002/eqe.4290050306.

72. Federal Emergency Management Agency (FEMA), *Seismic Performance Assessment of Buildings, Volume 1 and 2 (FEMA P-58)* (Applied Technology Council (ATC), 2012), prepared by ATC for the Federal Emergency Management Agency, https://www.atcouncil.org/pdfs/ATC-58-1/FEMAP-58_Volume1_Pre-ReleaseAugust2012.pdf.

73. G. A. MacRae, Y. Kimura, and C. Roeder, "Effect of Column Stiffness on Braced Frame Seismic Behavior," *Journal of Structural Engineering* 130 (2004): 381–391, https://doi.org/10.1061/(ASCE)0733-9445(2004)130:3(381).

74. B. Qu, F. Sanchez-Zamora, and M. Pollino, "Mitigation of Inter-Story Drift Concentration in Multi-Story Steel Concentrically Braced Frames Through Implementation of Rocking Cores," *Engineering Structures* 70 (2014): 208–217, https://doi.org/10.1016/j.engstruct.2014.03.032.

75. M. F. Vassiliou and N. Makris, "Estimating Time Scales and Length Scales in Pulselike Earthquake Acceleration Records With Wavelet Anal-

ysis," *Bulletin of the Seismological Society of America* 101, no. 2 (2011): 596–618, https://doi.org/10.1785/0120090387.

76. G. P. Mavroeidis and A. S. Papageorgiou, "A Mathematical Representation of Near-Fault Ground Motions," *Bulletin of the Seismological Society of America* 93, no. 3 (2003): 1099–1131, https://doi.org/10.1785/0120020100.

77. G. P. Mavroeidis, G. Dong, and A. S. Papageorgiou, "Near-Fault Ground Motions, and the Response of Elastic and Inelastic Single-Degree-of-Freedom (SDOF) Systems," *Earthquake Engineering & Structural Dynamics* 33, no. 9 (2004): 1023–1049, https://doi.org/10.1002/eqe.391.

78. E. Efthymiou and N. Makris, "Pulse-Period–Moment-Magnitude Relations Derived With Wavelet Analysis and Their Relevance to Estimate Structural Deformations," *Earthquake Engineering & Structural Dynamics* 51 (2022): 1636–1656, https://doi.org/10.1002/eqe.3674.